An Aerodynamic Analysis of the Changes in Airflow Between 2021 and 2022 Formula One Cars

Name: James Clay

Date: 04/05/2023

Supervisor: William Prowry

Words: 9198

This report is submitted in partial fulfilment of the requirements for the Meng Aeronautics and Astronautics / Aerodynamics program, Faculty of Engineering and Physical Sciences, University of Southampton.

Declaration

I, James Clay declare that this thesis and the work presented in it are my own and has been generated by me as the result of my own original research.

I confirm that:

1. This work was done wholly or mainly while in candidature for a degree at this University;

2. Where any part of this thesis has previously been submitted for any other qualification at this University or any other institution, this has been clearly stated;

3. Where I have consulted the published work of others, this is always clearly attributed;

4. Where I have quoted from the work of others, the source is always given. With the exception of such quotations, this thesis is entirely my own work;

5. I have acknowledged all main sources of help;

6. Where the thesis is based on work done by myself jointly with others, I have made clear exactly what was done by others and what I have contributed myself;

7. None of this work has been published before submission

Acknowledgements

I want to thank my supervisor, Dr William Prowry, for his help and guidance with this project. I would also like to thank my friends and family for their support over the months this investigation took place.

James Clay

Abstract

This project analysed the external flow around a modern Formula One car. It compared the differences between 2021 and 2022 and examined the changes' effectiveness and whether the changes succeeded in completing their objectives.

The experiment was conducted using Siemens Simcenter Star-CCM+ for CFD simulations. From the simulations, flow patterns were analysed, specifically those which showed high levels of vorticity and turbulence. From these results, it was concluded that the regulation changes had achieved the objectives they set out very well but not quite perfectly.

Table of Contents

1 Introduction

1.1 Glossary of Symbols and Abbreviations

FIA	Federation Internationale de l'Automobile.
CFD	Computational Fluid Dynamics.
CAD	Computer Aided Design.
HPC	High Performance Computer.
C_L	Coefficient of lift.
C_D	Coefficient of drag.
C_p	Coefficient of pressure.
u	Flow velocity.
ρ	Density.
p	Pressure.
μ	Dynamic viscosity.
μ_t	Turbulent viscosity.
ν	Kinematic viscosity.
f	External forces.
g	Acceleration due to gravity.
μ_{max}	Maximum coefficient of friction.
k	Turbulent kinetic energy.
ε	Turbulent dissipation rate.
G_k	Generation of turbulent kinetic energy due to the mean velocity gradients.
G_b	Generation of turbulent kinetic energy due to buoyancy.
Y_M	Fluctuating dilation in compressible turbulence to the overall dissipation rate.
σ	Prandtl number.
S	Source terms.
$y+$	Non-dimensional wall distance.
$u+$	Non-dimensional velocity term.

1.2 Project Aim

This project aims to simulate the flow around a Formula One car and analyse the effect of a regulation change on the flow.

1.3 Project Objectives

The objectives of this project are:

- Analyse relevant theory and apply it to explain and understand the roles of aerodynamic devices on a Formula One car.
- Collect data using CFD on both a 2021 and 2022 car model.
- Compare the 2 data sets to show the effects of the regulation change.

1.4 Motivation for Project

The primary motivation for this project comes from a lack of modern research into Formula One aerodynamics. As will be shown later in the report, the modern Formula One car is one of the most aerodynamically complex car designs ever, yet very little research is available from the last ~15 years.

The 2021/2022 regulation change was chosen because it aims to combat arguably F1's biggest problem: turbulence. Turbulence has reduced the quality of racing in F1 due to it limiting the performance of cars following closely behind one another. This problem needs to be addressed for more overtakes, ultimately increasing fan enjoyment of the sport and therefore allowing the sport to prosper both in the eyes of the fans and shareholders.

This report will build an understanding of the methods used in 2022 to reduce turbulence and analyse their effectiveness to build a platform to develop new and improved methods to reduce turbulence further.

2 Background Information

This section will contain an overview of the relevant aerodynamic ideas used throughout this project and introduce the concept of Formula One aerodynamics, specifically, how the aerodynamic parts work and how they changed between 2021 and 2022.

2.1 Aerodynamic Theory

This section is an overview of the Navier Stokes equations, Coanda effect and vortex generation, three fundamental concepts used throughout this project.

2.1.1 Navier-Stokes Equations

The Navier-Stokes equations are a set of momentum-based equations which describe the motion of fluids. The Navier-Stokes equations are expressed as a system of equations that relate the rate of change of velocity, pressure, and density to the forces acting on the fluid. The equations are derived from the principles of conservation of mass, momentum, and energy. They can be written in several different forms, but a common form is:

$$\frac{\partial \rho}{\partial t} + \nabla \cdot (\rho u) = 0 \qquad Eq.\ 1$$

$$\rho\left(\frac{\partial u}{\partial t} + u \cdot \nabla u\right) = -\nabla p + \mu \nabla^2 u + f \qquad Eq.\ 2$$

Where ∇ is the del operator such that $\nabla = \frac{\partial}{\partial x} + \frac{\partial}{\partial y} + \frac{\partial}{\partial z}$, ρ is the density of the fluid, $\mathbf{u}$ is the velocity vector, p is the pressure, μ is the dynamic viscosity, and $\mathbf{f}$ is any external forces acting on the fluid.

Eq. 1 is the continuity equation. It states that the rate of change of the density of the fluid is equal to the divergence of the mass flux density.

Eq. 2 is the momentum equation. It states that the rate of change of momentum of the fluid is equal to the sum of the forces acting on it, including pressure, viscosity, and external forces.

The Navier-Stokes equations are notoriously difficult to solve analytically, especially for turbulent flows, which are characterised by chaotic and unpredictable motion like the ones encountered in this project. This is why aerodynamicists use CFD software, which uses large amounts of computational power to solve these equations. CFD will be used for the data-gathering part of this project, so an understanding of these equations is needed.

2.1.2 Coanda Effect

The Coanda effect is a phenomenon in fluid dynamics where a fluid flowing over a curved surface follows the contour of the surface instead of continuing to flow in a straight line.

The Coanda effect occurs when a high-speed fluid flow is directed at a curved surface. Instead of continuing in a straight line, the flow adheres to the surface and follows its curvature. This happens because the fluid molecules near the surface are in a boundary layer of low velocity due to the viscous effects near the surface boundary. This causes the fluid to adhere to the surface and follow its curvature (Camuffo, 2019).

The critical point is that the higher the energy of the flow, the more likely the flow is to stay attached. This is a crucial concept in Formula One aerodynamics, as will be seen later, as many techniques are used to keep the flow attached using the Coanda effect.

2.1.3 Vortex Generation

Vortices are a fundamental fluid structure commonly encountered in this project. In the context of aerodynamics, a vortex is a swirling motion of air generated by an object's movement through the air. Specifically, in the case of a wing, vortices are generated at the wingtips when air flows from the wing's high-pressure side to the wing's low-pressure side. This effect can better be seen in figure 1 below:

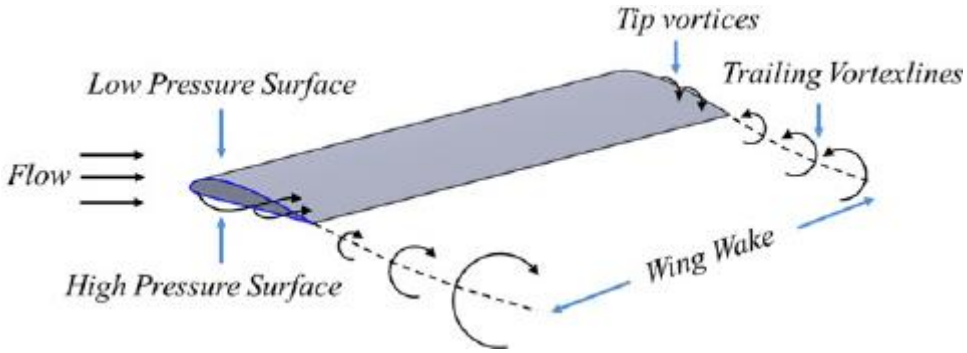

Figure 1. A graphical demonstration of how vortices are generated. (Guha et al., 2015)

2.2 Formula One Aerodynamic Principals

In the sport of Formula One, engineers must innovate new technologies to produce the fastest lap times out on track. In the late 1960s (see figure 2), utilising aerodynamics was recognised as an opportunity to improve performance

and reduce lap times. Ever since, Formula One has been home to the most advanced race car aerodynamics, even in 2021.

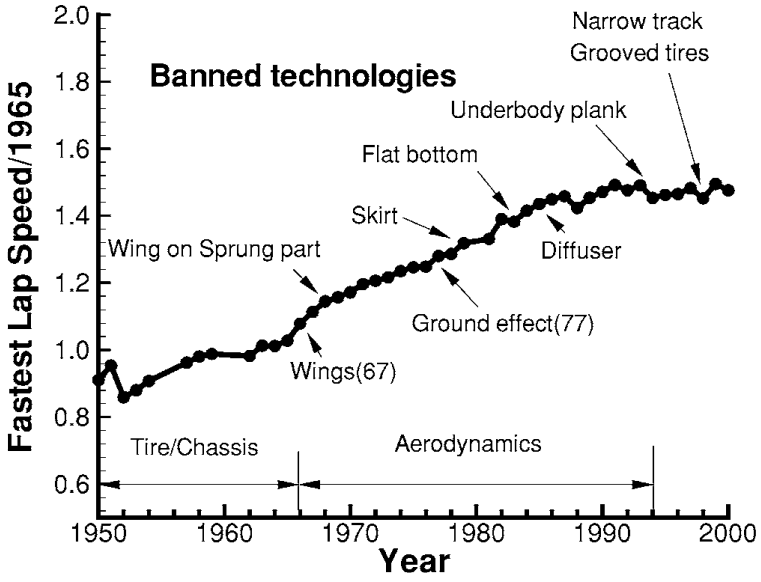

Figure 2. Graph showing the impact of aerodynamics on lap time. (X. Zhang et al., 2006)

The main aim of using aerodynamics on race cars is to generate a high level of downforce (negative lift) while producing minimal drag. The importance of aerodynamics is easy to explain. Given a fixed distance, the average speed of a car determines the time it takes to complete a circuit. However, over a closed circuit, it is the change of velocity, i.e., acceleration, which is the deciding factor in determining the speed performance of the car. A race car's braking, accelerating, and cornering performance are the limiting factors in deciding a car's performance. A simple expression can illustrate the acceleration of a car:

$$Acceleration = g \times \mu_{max} + \frac{Downforce \times \mu_{max}}{M} \qquad \text{Eq. 3}$$

Where g is the acceleration due to gravity, μ_{max} is the maximum coefficient of friction of the tyre, and M is the mass associated with that tyre (X. Zhang et al., 2006).

This equation and figure 3 clearly show how an increase in downforce generated can improve the performance of a race car by improving its acceleration.

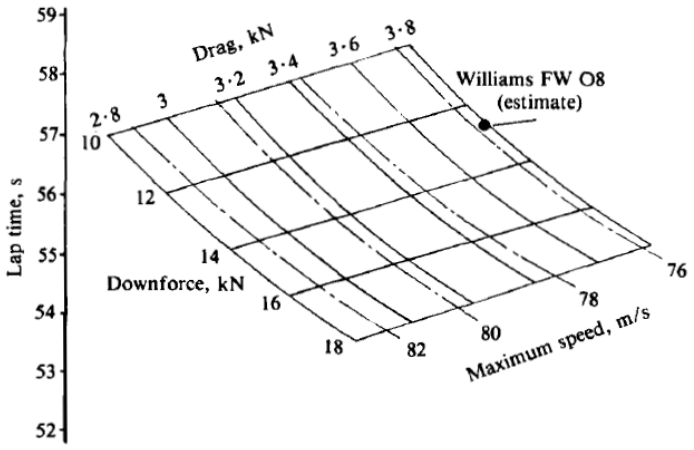

Figure 3. Variation of lap time with aerodynamic downforce and drag for a Formula One racing car. (Dominy & Dominy, 1984)

2.2.1 Technical Regulations

The sport of Formula One has a governing set of technical regulations set by the Federation Internationale de l'Automobile (FIA), which the teams must design their cars to for them to be deemed legal and allowed to compete in the races.

The technical regulations that governed up until the end of 2021 (Fédération Internationale de l'Automobile, 2017) have a clear emphasis on designing overbody aerodynamics (aerofoils and other winglets) instead of using underfloor aerodynamics (acceleration of air underneath the car). The biggest problem with this was how turbulence (known as "dirty air") affected the following cars due to decreased efficiency in the following car's aerodynamics.

Formula One cars produce a wake like any body in a flow. Due to the aerodynamic nature of the car, this wake is highly turbulent and unsteady. The problem with this is that turbulent wakes reduce the lift of pre-stall aerofoils (Z. Zhang et al., 2022). This meant that any car following another was experiencing a loss in grip from being behind another car, leading to less overtaking and a change in the technical regulations for 2022. It was estimated that the 2021 cars lost 35% of their downforce by following 20 metres behind another car, whereas the 2022 regulations aimed to reduce that to only 4% (Kanal, 2022). The wake will also contain a lot of vortices and eddies, which can be seen in figure 4, and the problem with this is that they are unpredictable, which means the performance of the aerofoils will be unpredictable in turn.

The final problem is that the flow in the wake will be less energised and have a lower velocity. This reduces lift because aerofoils in lower velocity flows produce less lift. This idea of lower energy flow in the wake is also why the slipstream effect exists because lower flow velocity also reduces the effect of drag. This property exists in the wake of

most bodies no matter how they are designed aerodynamically and so it cannot be affected much by changing the car design. This might be for the best because, as previously mentioned, this lower velocity flow is what creates slipstream, which is a valuable tool when trying to overtake another car.

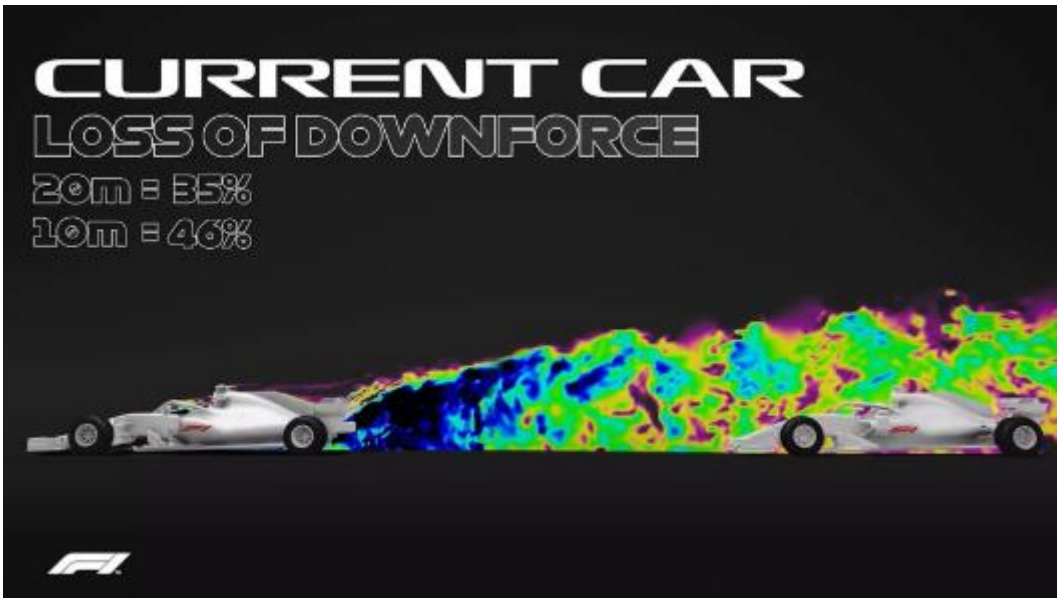

Figure 4. A visual indicator of the turbulent nature of the wake of the 2021 Formula One car. (Auto Leader, n.d.)

To reduce the effect of the wake, Formula One decided to increase emphasis on ground effect aerodynamics in the 2022 regulations. This is where the car uses its proximity to the ground to create an area of low pressure under the car to produce massive amounts of downforce. This will boost overtaking because this method of producing downforce is less affected by being in the turbulent wake of another car behind, allowing them to follow closer and be in range to overtake (Hughes, 2022).

2.2.2 Tyre Wake

The wake of a tyre is a significant factor in designing race cars. The wake of a tyre is incredibly chaotic, as shown in figure 5. If the 2D case is considered, tyres act like circles in a flow where separation occurs just over the crown of the tyre, creating a separation bubble behind the tyre, which is turbulent and then that turbulent flow travels downstream and can disrupt the aerodynamics.

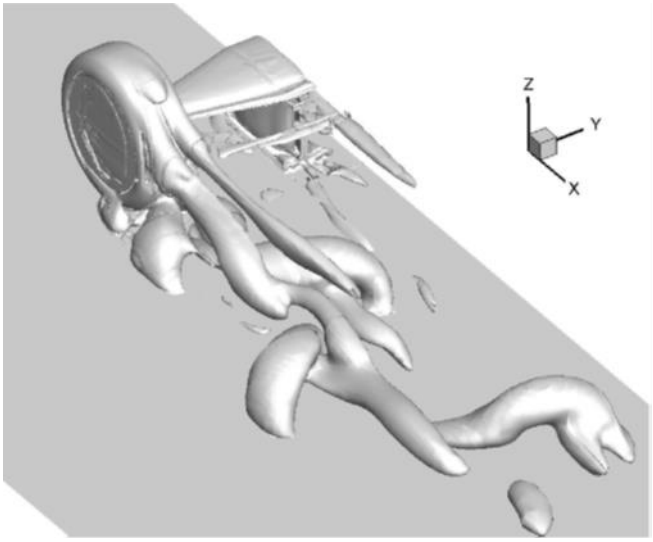

Figure 5. The wake of an isolated tyre. (Croner et al., 2012)

Additionally, the surface of the tyre is rough, and it is spinning towards the oncoming flow, which can cause the boundary layer to trip early, causing the flow to detach and become turbulent even further upstream than a smooth, fixed circular object.

Previously, designers have tried to push this wake outwards (outwash) rather than allowing it to get sucked in towards the rear of the car and disturb the aerodynamics. This meant the following car had to deal with this disturbed air instead, further reducing the performance (Scarborough, 2021).

2.2.3 Vortices and Flow Attachment

Vortices are a large part of how Formula One designers control the flow of the air around the car. Typically, in aerodynamics, vortex generation is seen as a harmful product of geometry because of the increased drag produced; however, in race car aerodynamics, vortices are used both to create the aforementioned outwash effect as well as to keep high speed, laminar flow permanently attached to the car.

However, as discussed previously, vortices in the wake of the car provide an unpredictable airflow for the following car. This means that while large amounts of vortex generation might be optimal for a car in front, the following car will suffer because of those vortices.

2.3 Formula One Aerodynamic Components

This section will introduce various key aerodynamic components of 2021 Formula One cars, how they work and why they are helpful.

2.3.1 Front Wing

Figure 6. Red Bull Racing RB16-B. (Red Bull Racing, 2021)

The front-most and arguably most crucial component of the car is the front wing which is used to create downforce to generate front turn-in. As seen in figure 6, 2021 front wings are made up of multiple elements. The purpose of this is to introduce a slot gap between those elements. A slot gap is the pocket of air between 2 aerofoils where high-pressure flow from one aerofoil is fed to the lower surface of the second aerofoil to keep the flow attached. The wings used on a Formula One car have a very low aspect ratio, so they must be placed at high angles of attack to produce large amounts of downforce; however, placing them at these angles has a significant chance of stalling the wing, so slot gaps are used. Figure 7 below shows how this bleeding effect is performed:

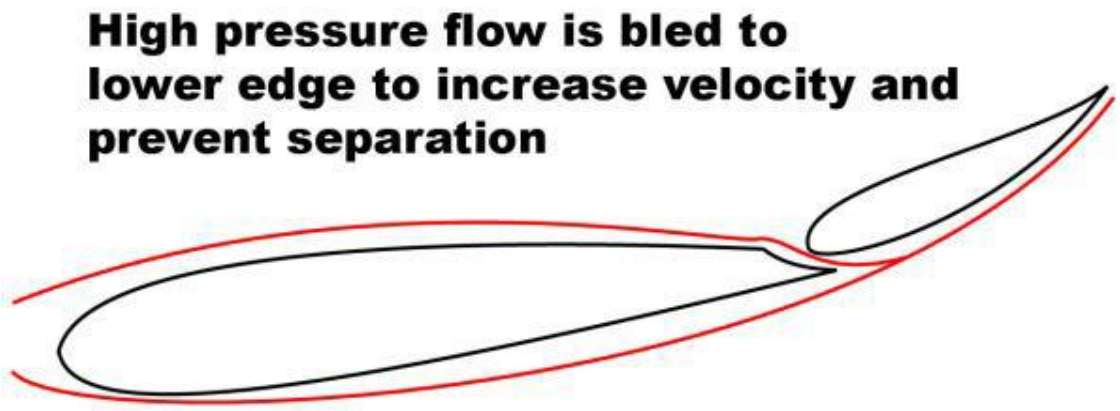

Figure 7. Visual explanation of how slot gaps work. (McBeath, 1999)

The endplate is used to concentrate the vortex into one tip vortex instead of the vortices that would be usually shed by the wing due to the pressure difference. This allows the flow of the mainplane of the wing to stay attached better and improves performance. The concentrated vortex is also much more effective at encouraging outwash by mixing with the turbulent tyre wake rather than multiple vortices, which may interfere with each other.

2.3.2 Rear Wing

The rear wing is much more simplified than the front wing (see figure 8). This is because the wake of the rear wing is of little concern to the engineers since there are no components downstream to worry about hindering the performance. It uses a multi-element system with slot gaps for the same reasons as the front wing. The only other design choices are made to reduce drag; however, there is no attempt by the designers

to control the flow using the rear wing. The rear wing has a massive impact on the performance of the car not only by increasing cornering performance but since Formula One cars are rear-wheel drive, the rear tyres are the only ones providing a driving force, so maintaining rear grip is crucial to provide optimal acceleration on corner exit.

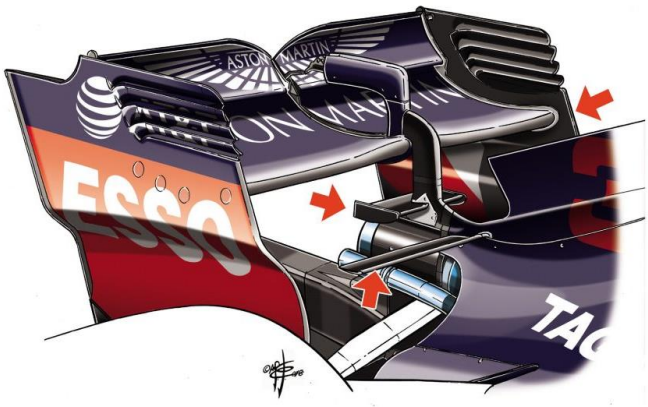

Figure 8. A modern Formula One rear wing design. (Formula One, 2018)

2.3.3 Bargeboards

The final major overbody aerodynamic component is the bargeboard area. The bargeboards are a complex collection of winglets located in front of the sidepod air inlets just behind the tyre. However, Table 1 shows that despite all their complexity, the bargeboards do not produce even 2% of the car's total downforce. Instead, figure 9 shows how the bargeboards' main purpose is to manipulate the airflow downstream to boost the components further along the car.

Table 1 Relative downforce and drag contributions of different parts of a Formula One car. (Guerrero & Castilla, 2020)

Elements	Downforce Contribution (%)	Drag Contribution (%)
Bargeboards and vanes	-1.71	+2.97
Bodywork	+21.10	+10.70
Front suspension	+2.36	+2.88
Front Tires	+2.94	+10.30
Front Wing	-22.84	+12.69
Rear suspension	-0.40	+3.93
Rear tires	+1.42	+20.06
Rear wing	-35.46	+20.38
Underbody	-61.09	+15.05
Others	-6.65	+1

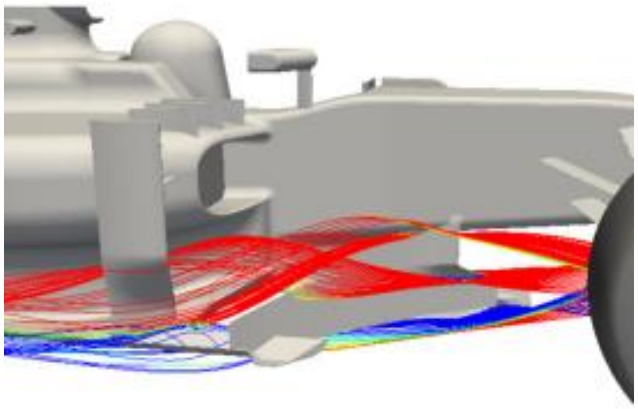

Figure 9. Streamlines showing airflow around the bargeboards. (Umberto Ravelli & Marco Savini, 2018)

Bargeboards are a large contributor to the outwash effect. They help guide vortices from the inboard portion of the front wing, which mixes with the tyre flow, which can be seen by the red streamlines in figure 9. The bargeboards also generate even more vortices as well. These vortices will eventually spill out behind the car, further increasing the turbulence of the wake just like those generated by the front wing.

Another large role of the bargeboards is to direct the vortices to the edge of the floor. This can be seen by the blue-coloured streams in figure 9. This is done to minimise air from under the floor spilling out, reducing the efficiency of that part and is crucial to maximising performance.

2.3.4 Underbody

Table 1 also shows that despite being heavily restricted in design, the underfloor is the largest producer of downforce in the old regulations when it was essentially just a flat plane (61%). The underfloor generates downforce using a phenomenon known as ground effect. It works by having high-velocity airflow travel underneath the floor of the car. Then, the diffuser provides a gradual transition of this airflow to the slower freestream at its exit. The diverging area of the diffuser creates this transition by easing the low-pressure airflow at the inlet to the higher atmospheric pressure at the exit.

2.4 2022 Changes

This section will illustrate how the 2022 rules will change the previously mentioned geometry and why this is done in the context of limiting the dirty air effect.

2.4.1 Front Wing

Alongside the endplate vortex mentioned in 2.3.1, there is another vortex generated by the 2021 front wings. This was the Y250 vortex. It is generated by the inner wingtips of the front wing. It is illustrated perfectly in figure 10. This was a session where the humidity was high enough that the vortex could be seen by the naked eye.

Figure 10. The Y250 vortex, visible from a session in 2013. (wickedender, 2013)

However, looking at figure 11, in 2022, the winglets are attached to the nose cone completely to remove the concentrated Y250 vortex entirely. This vortex was normally directed towards the bargeboards to be turned outboard and mixed with the tyre wake like the tip vortex to encourage outwash. It was a vortex that was difficult to control when in a disturbed flow because it was less predictable, just another way that the following

car suffered. The removal of this vortex is one of the ways F1 are trying to reduce outwash and improve the performance of the following cars.

Figure 11. A comparison between the 2021 and 2022 front wing designs. (Hughes & Piola, 2022)

Visually, the 2022 wing is much simpler and differently shaped than its 2021 counterpart. This will reduce the total downforce generated; however, it means that a reduction in front wing efficiency will be a lower proportion of total downforce lost compared to running in undisturbed flow. This will keep the car balance more constant since the front wing is the front-most device, and it has a great effect on the aerodynamic centre of the car.

The difference in the shaping of the aerofoils is also key for another reason. This is because they have been designed in a way that should reduce the amount of turbulence shed behind the front wing and further downstream.

2.4.2 Rear Wing

As can be seen in figure 12, the rear wing has become one connected piece in 2022. Before, there were very concentrated tip vortices because the high-pressure air would spill over the top of the endplates and mix with the lower-pressure air on the other side. This effect would create a swirling, turbulent flow behind the rear wing which would interfere with the car behind. The simplified wing, like at the front, does also produce less downforce, so it too will be less affected by the lack of clean air when following another car, thus further improving the car's ability to follow.

Figure 12. A comparison of the 2021 and 2022 rear wing designs. (Reynolds, 2021)

The new design also improves the upwash of the air coming off the car, thus allowing the car behind to essentially drive underneath the turbulent wake to reduce the reduction in downforce. It does this in combination with the beam wing that surrounds the exhaust, which pushes the air from under the car upwards to reduce the pressure under the car whilst increasing upwash.

2.4.3 Underfloor

As seen in figure 13 a), the 2022 floors are using a 3D geometry instead of a flat plane. This is to utilise "Venturi tunnels" under the car, which use the Venturi effect and Bernoulli's principle. They have a large inlet to collect large amounts of air and then constrict the area under the car, accelerating the air, due to conservation of mass, towards the outlet where the flow then expands and creates a region of low pressure which is demonstrated in figure 13 b) which shows how ground effect was used when it was last incorporated into Formula One.

The outlet is further forward than the previous generation. This is to shift the centre of pressure forward to help with the reduction of downforce from the front wing, and it will limit the front sliding when in turbulence since a higher proportion of the downforce is coming from the underfloor.

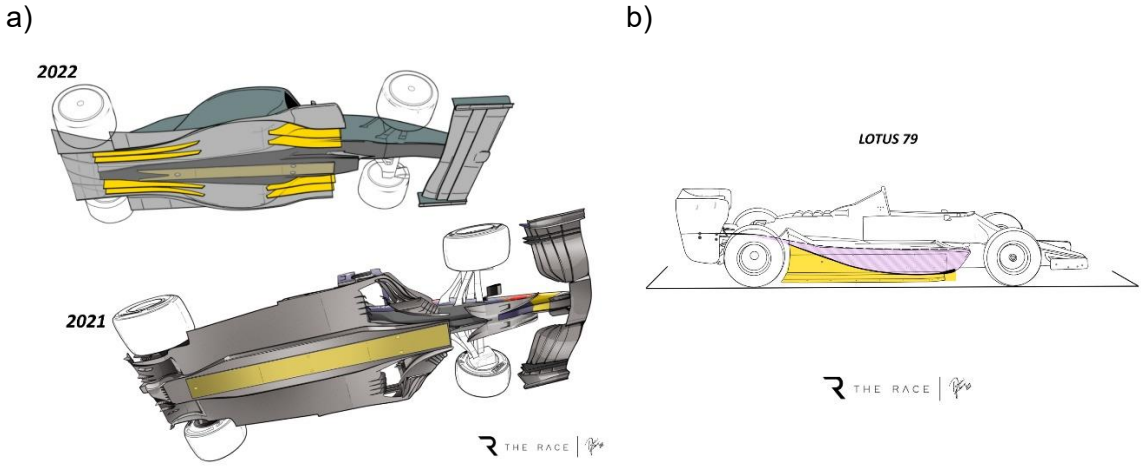

Figure 13. Drawings of Formula One car underfloors. a) A comparison of 2021 and 2022 floors. b) A drawing of how ground effect cars work. (Anderson, 2022)

2.4.4 New Devices

2022 brings with it two new devices around the tyres. These are winglets above the front tyres as well as covers over the wheel rims. These devices are designed to help manage the wake of the tyres. The wheel rims have also been increased from a 13-inch to an 18-inch diameter.

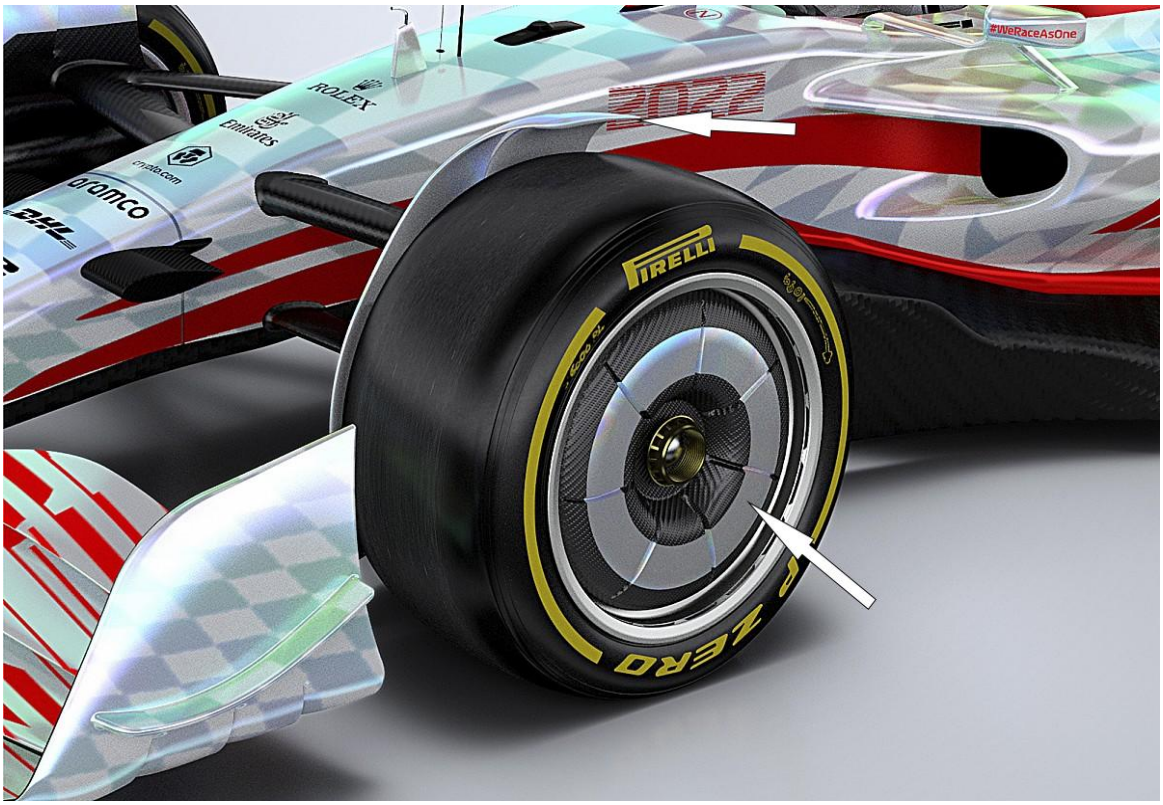

Figure 14. Image of the 2022 front tyre with arrows pointing to the new devices. (Anon., 2021)

The winglet above the tyre is designed to encourage the tyre wake upwards. This is a part of Formula One's desire to encourage upwash to limit the level of turbulence experienced by the car behind.

The rim covers are a device which aims to decrease separation to reduce the size of the separation bubble and, therefore, the intensity of the turbulence in the wake of the tyre. It does this by providing a smoother surface on the inside of the tyre, which should help keep the flow more attached as well as stop air from being affected by objects such as the wheel spokes and brake discs.

Finally, the change to 18-inch rims means that less of the wheel is made of tyre. This is important because the tyre flexes and deforms much more under load than the wheel does. This means that any flow shed off the tyre will be more consistent than those shed by previous generations of tyres since the shape of the tyre will change less over time. However, this effect will not be possible to be modelled in this project, so the effectiveness of this change cannot be analysed in this report.

3 Simulation Methodology

3.1 Introduction

The heart of this project involves running computational fluid dynamics (CFD) simulations in the program Siemens Simcenter STAR-CCM+ for two different geometries: 2021 and 2022. There were many obstacles between starting this process and obtaining the final results, and these will be discussed in detail in this section alongside the methodology used.

3.2 CFD Software

STAR-CCM+ was chosen as the software for this project because it was the one that there was the most experience with, but it is also an extremely powerful piece of software that is used widely in the aerospace industry and is used by many motorsport teams.

STAR-CCM+, like any CFD software, applies the Navier-Stokes equations to geometries at a far higher computational speed than humans ever could by hand. To get to a final solution, the software applies an iterative method to converge on a solution for the flow properties of the geometry.

The simulations could be run either on the University of Southampton High Performance Computer (HPC) or a local machine. In this case, the simulations would be run on a local machine with the following specifications:

- CPU: AMD Ryzen 5950x 4.8GHz 16 core/ 32 thread processor
- RAM: 32GB 2666MHz memory
- GPU: Nvidia RTX 3080 Founders Edition

3.3 Geometry

The geometries were obtained online from the same designer. This was done to increase consistency between the meshes in areas such as the method in which they were made and the level of detail. The geometry was purchased under the TurboSquid 3D Model License, which permits the use of models for educational purposes, including coursework.

The two geometries are shown in the figures below and were the "3D Formula 1 Season 2022 F1 Race Car Concept model" and "3D Grey Cat F1 GC16B 2021 Formula 1(1)" purchased from the creator OpticalDreamSoft (OpticalDreamSoft, n.d.). The 2022 model was chosen as it was based on the 2022 design made directly by the FIA, which meant it demonstrates the exact ideas the rule makers wanted to implement and eliminates any interpretations of the rules. The 2021 car was chosen as it is based on the 2021 RB16-B,

which led Max Verstappen to the 2021 World Drivers Championship and won the most races of any car on the grid, meaning it is a well-designed car which makes the most of the 2021 regulations.

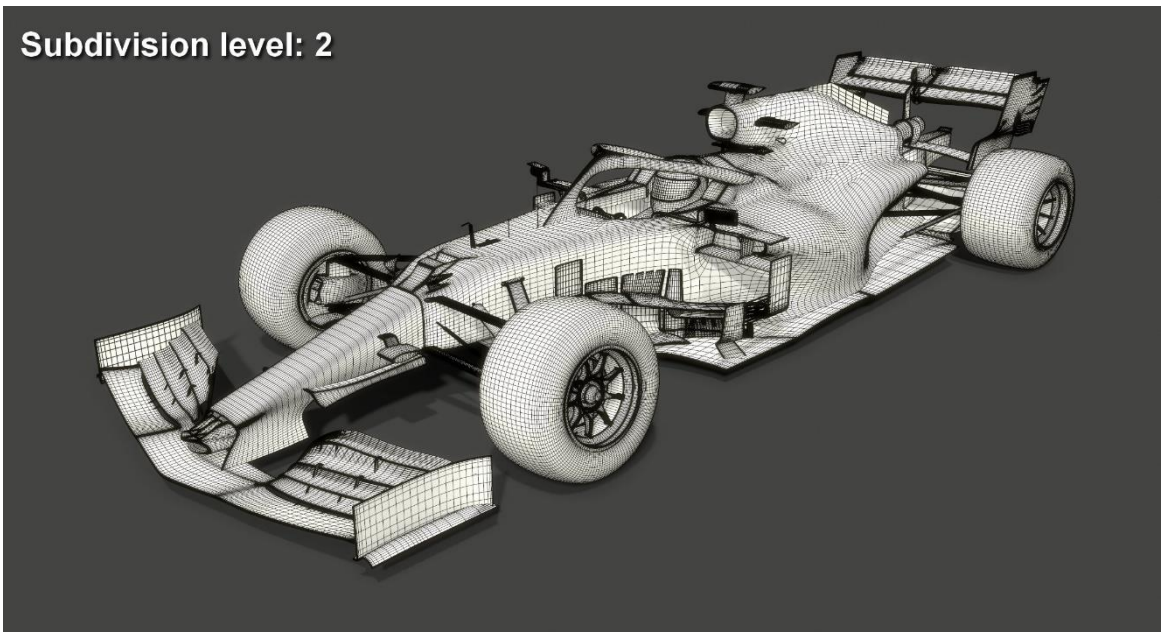

Figure 15. 2021 geometry which was purchased. (OpticalDreamSoft, n.d.)

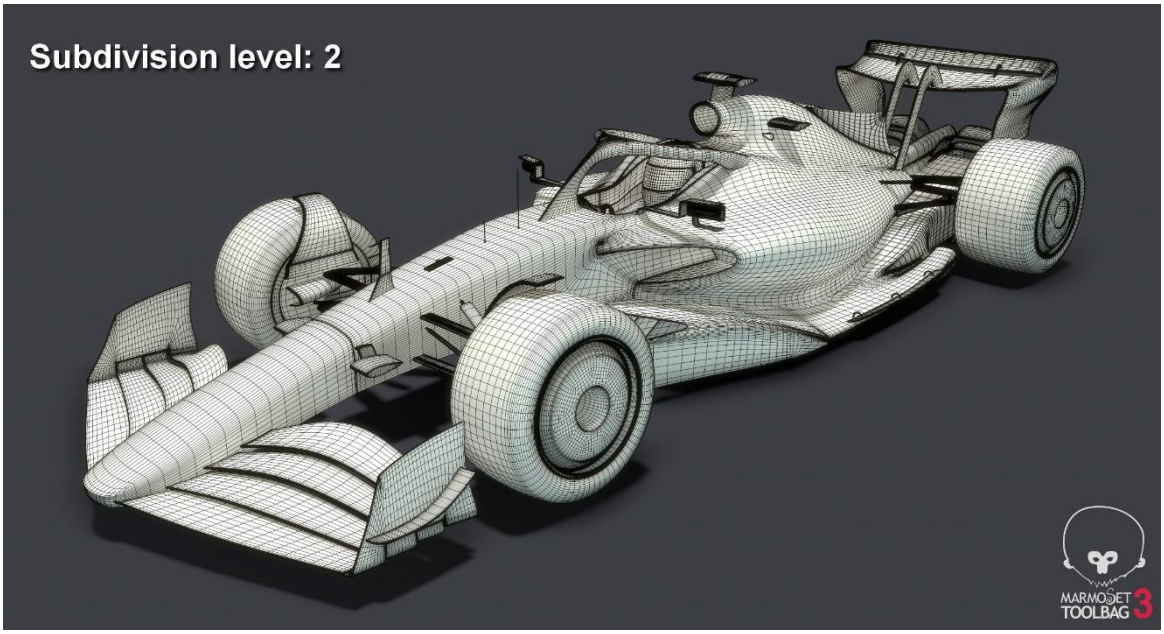

Figure 16. 2022 geometry which was purchased. (OpticalDreamSoft, n.d.)

Once downloaded, the models were imported into a computer aided design software (CAD): Autodesk Fusion 360. Fusion 360 was chosen because it has very useful meshing tools. The reason this is useful is that the geometries came as mesh geometries and not solid bodies. Therefore, the first step was opening the purchased files into Fusion 360, repairing the mesh, and converting it to a solid body.

This was the first limitation that came with this project. The meshes which were purchased were not designed by engineers for CFD simulations. They are designed by 3D model designers for movies, games, and other creative outlets. However, there is no way to obtain the files created by Formula One engineers, and these models were clearly made with close attention to detail. This was the main reason why this project would be a qualitative analysis rather than a quantitative one, because the geometry can never be classed as completely accurate.

The problem with the meshes lies in the fact that some of the volumes are not closed, and there are holes in the surface. This means they would have infinite volume when trying to convert to a solid body which would not work. Fortunately, Fusion 360 has a very good mesh repair tool which seamlessly repairs small holes in the mesh, and then it has another tool which converts the now sealed body into a solid.

The next problem was the complexity of the model. The geometry was smoothened by the creator through the process of subdivision (the process where a model's polygons are split whilst keeping the existing shape), which greatly increased the size of the geometry files. The issue with this was importing the geometry into STAR-CCM+ as well as an increase in computational time when completing the solution. To resolve this, the model was simplified. The simplifications included the removal of suspension, aerials and pitot tubes, steering wheel, seat, and television cameras. This was because these parts are not key to the investigation and will increase computation time.

The other simplifications performed took advantage of symmetry. To save time on computation, CFD simulations of symmetrical models only solve for half the model, and then this can be copied and flipped over the plane of symmetry to provide a whole result in analysis. This meant that parts of the car on one side could be deleted. This would not save solver time; however, it would reduce the size making importing the file into Star-CCM+ much easier. Many of the parts that were only on one side were deleted until the two following geometries remained and could be imported into Star-CCM+.

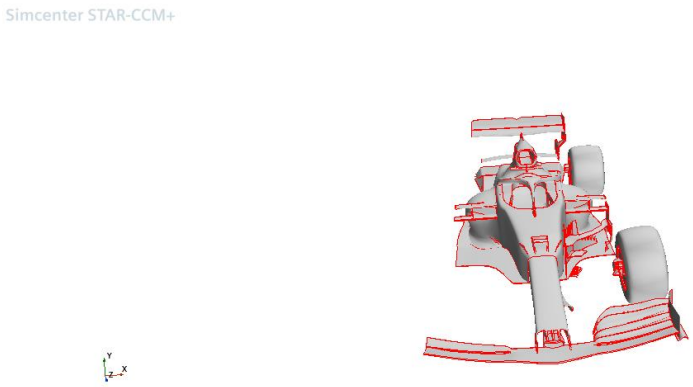

Figure 17. 2021 Geometry that was imported into Star-CCM+.

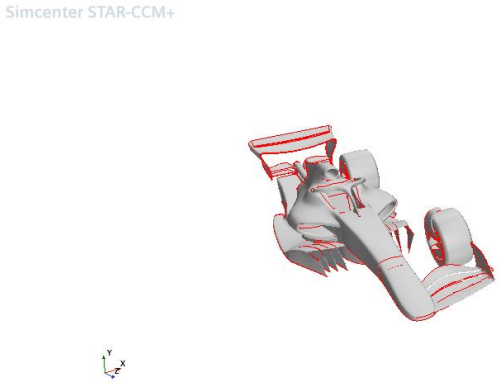

Figure 18. 2022 Geometry that was imported into Star-CCM+.

3.4 Solver Setup

For the following parts of section 3, only the 2022 geometry will be mentioned unless stated otherwise. However, the steps were identical for the 2021 geometry, as the exact same simulation environment was used for both geometries.

Once imported into Star-CCM+, the geometry was placed into a simulation configuration shown in figure 14 below. The control volume around the geometry was made in Star-CCM+ with a length, height, and width of 50 m, 7.5 m, and 7.5 m, respectively. The box was split by patch into a floor, symmetry plane, walls, inlet, and outlet, as can be seen in figure 19.

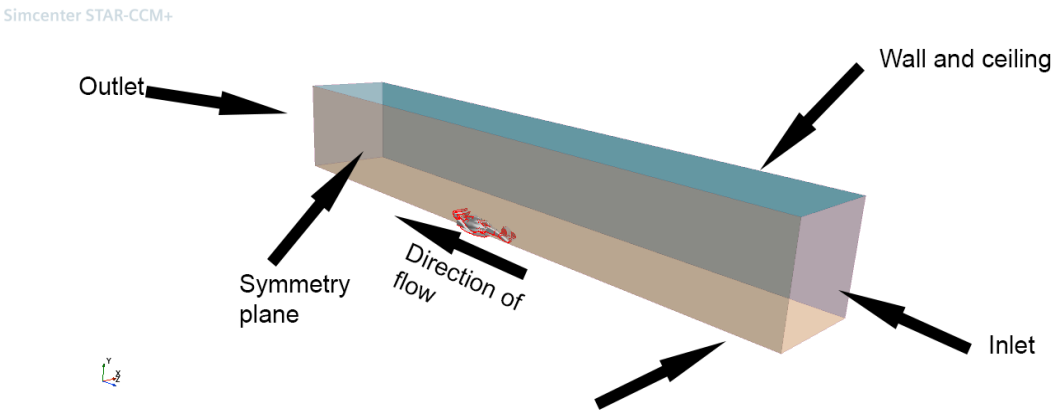

Figure 19. Control volume setup in Star-CCM+.

The box was placed with the symmetry plane cutting through the middle of the geometry with the mid-line of the plane along the z-axis intersecting the origin of the geometry. The box was also positioned by raising the floor by 1 cm increments until the floor intersected the bottom of the tyre geometry to create a seal between the tyre and the floor.

The box dimensions were chosen to increase the space between the geometry and the boundaries. This was done for multiple reasons: firstly, it was to reduce the impact of any unsteadiness in the flow from the inlet downstream of the model. Secondly, it was done to minimise the effect of any flow reversal at the outlet. Finally, it was to reduce the impact of the side wall and ceiling since, in the real world, there would not be walls there on the track.

The final step is to subtract the geometry from the control volume. This is done so that Star-CCM+ can create a fluid volume to be used in the simulations. This step is performed by the native boolean subtract function in Star-CCM+.

3.5 Turbulence Model and Solver Settings

The CFD simulations in this project are all using a Reynold-Averaged Navier-Stokes (RANS) turbulence model. RANS models work by averaging the 3D Navier-Stokes equations over a long period to produce a set of averaged flow properties.

The specific RANS model being used is the k-epsilon realisable two-order model. The k-epsilon model is often the best model for external flow simulations rather than focusing on boundary layer flow which is the primary objective of this project. The realisable model was chosen because it gave better solution convergence than the base model, and the second-order model was used because it is often more accurate in its results.

One of the main drawbacks of this model is that it will produce a steady-state solution rather than a transient one. Given the expected level of turbulence in the solution, this is not the ideal solver type. However, the use of a steady-state solver will greatly reduce

computational time, which is far more crucial to the project and is a necessary compromise.

The k-epsilon model works by solving the Navier-Stokes equations as well as two transport equations (PDEs) which account for the historical effects like convection and diffusion of turbulent energy. As its namesake suggests, the two transported variables are turbulent kinetic energy (k) and turbulent dissipation rate (ε). The transport equations for the realisable model are as follows:

$$\frac{\partial}{\partial t}(\rho k) + \frac{\partial}{\partial x_j}(\rho k u_j) = \frac{\partial}{\partial x_j}\left[\left(\mu + \frac{\mu_t}{\sigma_k}\right)\frac{\partial k}{\partial x_j}\right] + G_k + G_b - \rho\epsilon - Y_M + S_k \quad \textit{Eq. 4}$$

$$\frac{\partial}{\partial t}(\rho \epsilon) + \frac{\partial}{\partial x_j}(\rho \epsilon u_j) = \frac{\partial}{\partial x_j}\left[\left(\mu + \frac{\mu_t}{\sigma_\epsilon}\right)\frac{\partial \epsilon}{\partial x_j}\right] + \rho C_{1\epsilon} S_\epsilon - \rho C_2 \frac{\epsilon^2}{k+\sqrt{\nu\epsilon}} + C_{1\epsilon}\frac{\epsilon}{k} C_{3\epsilon} G_b + S_\epsilon \quad \textit{Eq. 5}$$

Where P_k represents the generation of turbulent kinetic energy due to the mean velocity gradients, P_b is the generation of turbulent kinetic energy due to buoyancy. Y_M is the fluctuating dilation in compressible turbulence to the overall dissipation rate. $C_{1\epsilon}$, $C_{2\epsilon}$ and $C_{3\epsilon}$ are all constants. σ_k and σ_ε represent the turbulent Prandtl numbers for k and ε. S_ε and S_k are source terms which will be defined in the simulation, and all other terms take on their normal meanings (Ansys, 2009). The constants and Prandtl numbers were all left at their default values for this simulation as follows:

Table 2 Values for the constants in the transfer functions of the k-epsilon model.

Constant	Value
$C_{1\epsilon}$	1.44
$C_{2\epsilon}$	1.9
$C_{3\epsilon}$	0.09
σ_k	1
σ_ϵ	1.2

3.6 Boundary Conditions

After setting up the solver, the next step was setting the boundary conditions for the different regions of the control volume. The boundary types were set as follows:

Table 3 Table of simulation boundary conditions.

Boundary	Type
Floor	Wall
Inlet	Velocity Inlet
Outlet	Pressure Outlet

Walls	Wall
Symmetry Plane	Symmetry
Car Surface	Wall

The first main boundary conditions to set were the inlet conditions. Specifically, the flow velocity needed to be decided upon. The inlet velocity was set at 50 m/s. This value was decided because the average speed of the fastest lap of the 2021 USA Grand Prix was 55.98 m/s (Formula One, 2021), so the inlet was set at 50 m/s for a round value for easier calculations as well as being easier to recreate in a wind tunnel if there was ever an opportunity to validate these results using real-world measurements. The other inlet conditions to consider were the turbulence specification. By consulting previous literature, it was found that the turbulent length scale could be set to the wheelbase of the car because it represents the size of the largest eddy. The turbulent intensity was set at 0.15, as it was one of the values used by other investigations (Guerrero & Castilla, 2020).

The floor was set to a rolling floor since the road under the car on track would not be static, so the floor in the simulation needed to be moving too. It was set to move at 50 m/s along the negative z direction. Other trivial boundary conditions included: 0 pa at the pressure outlet and setting the wall and ceiling to a no-slip condition.

The final boundary condition was setting the wheel rotation speed. The wheels on the car would not be static, so that surface had to have an angular velocity value. This was calculated using the wheel diameter of 0.72 m and car velocity to determine that for the car to be driving at 50 m/s, the tyres must be rotating at 22.1 revolutions per second or 1327 RPM, with the centre of rotation being set at the centre of the wheel nut.

3.7 Initial Meshing

Before applying meshing, the subtracted geometry needed to be repaired. This problem was once again caused by the problems in the original models. There are many faces which are intersecting or low quality. Fortunately, there are many native surface repair tools within Star-CCM+, and by applying these to the problem areas alongside Star-CCM+'s surface diagnostics tools, the number of errors was reduced significantly, such that the surface was ready to be meshed.

Meshing was performed using Star-CCM+'s automated mesh operation. The volume mesh was generated using the trimmed cell mesher alongside the prism layer mesher. The mesher settings were kept at default for the global volume initially. However, there were custom finer settings applied to the main geometry and even finer settings applied to the main aerodynamic surfaces and wheels.

An important part of the mesh is the prism layer. This is a layer of cells around the surface walls. There are many parameters which control this part of the mesh, such as spacing, thickness and number of layers. This layer is important specifically in CFD simulations because it is a very fine layer at the boundary and therefore is used for resolving boundary layer flow and is crucial in obtaining reliable results.

3.8 Mesh Refinement

The simulation was run with the settings defined in the previous sections; however, this would only be the first of many runs before the final simulation. The reason for this was that after each run, the mesh would be adjusted and refined until there was no noticeable benefit to making the mesh finer and the wall y+ fell within an allowable range.

Wall y+ is a non-dimensional property which shows how close the first cell of the mesh is to the surface. It is useful because it is the main indicator of how well-resolved the boundary layer will be. For the k-epsilon model, the allowable range of y+ values is 30 to 300. This is because y+ falls within what is known as the "logarithmic law region". This is a region where logarithmic y+ is proportional to the non-dimensional velocity profile u+. The advantage of using the realisable k-epsilon model is that it is also valid for y+ values under 30, which makes the mesh refinement a lot easier.

As can be seen in the figure below, the mesh went through many iterations to arrive at the final y+ values. The main tool that was used to do this was adjusting the prism layer values in the mesher. To decrease y+, the first grid cell should be positioned closer to the wall, and to increase, do the opposite.

The other part of the mesh refinement process was much simpler. The mesh was made finer after each simulation until there was no noticeable difference in the results, as can be seen in the pressure contours shown in the figures below not being very different.

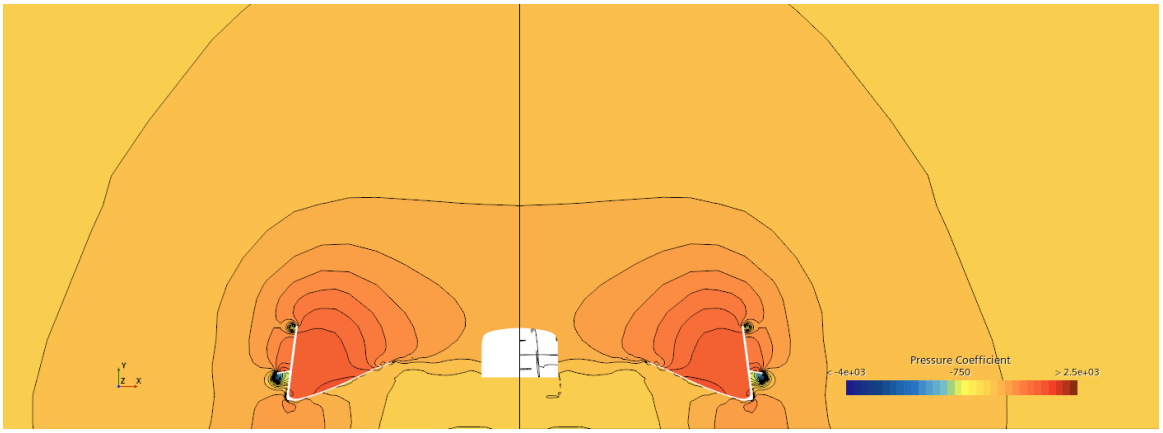

Figure 20. Cp plot of the 2022 car with a 7.8 million cell mesh.

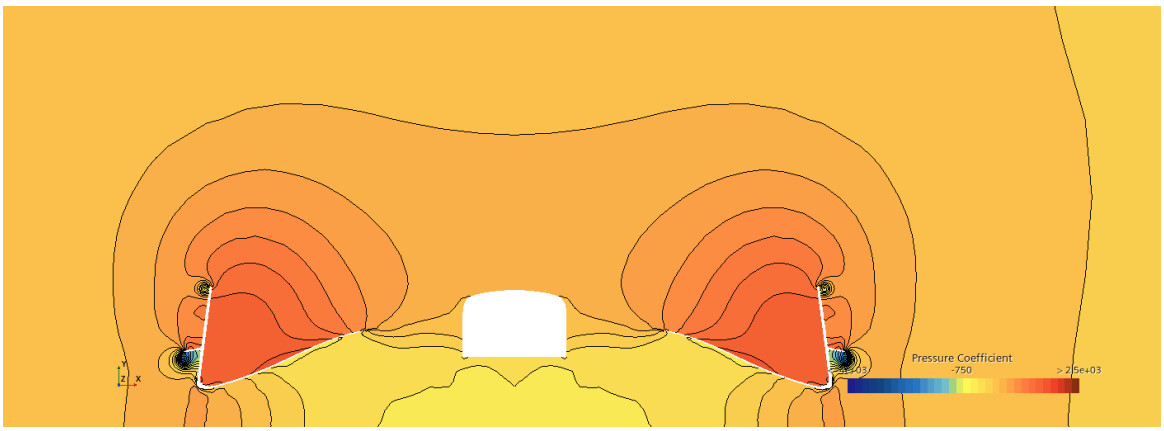

Figure 21. A Cp plot of the 2022 car with an 11.1 million cell mesh.

3.9 Summary of Settings

Below is a summary of solver settings and mesh settings that were used in the final simulations:

Table 4 Table of meshers used in the simulation.

Meshers
Surface remesher
Automatic Surface Repair
Trimmed Cell Mesher
Prism Layer Mesher

Table 5 Physics models used in the simulation.

Physics Models
Constant Density
Coupled Flow
Gas (Air)
3-Dimensional
Realisable k-epsilon
Two-Layer All Wall y+ Treatment
Steady
Gradients
Solution Interpolation
RANS

Table 6 Inlet initial conditions.

Setting	Value
Pressure	Constant Atmospheric (0 Pa)
Turbulence Intensity	0.35
Turbulence Specification	Intensity + Length Scale
Turbulent Length Scale	3.5 m
Turbulent Velocity Scale	1 m/s
Velocity Magnitude	50 m/s

Table 7 Global mesh settings

Setting	Value
Base size	0.5 m
Surface Growth Rate	Fast
Number of Prism Layers	2
Prism Layer Stretching	1.2
Prism Layer Total Thickness	15 mm
Volume Growth Rate	Medium

Table 8 Aerodynamic surfaces mesh settings.

Setting	Value
Base size	11 mm
Surface Growth Rate	Slow
Number of Prism Layers	10
Prism Layer Stretching	1.2
Prism Layer Total Thickness	30 mm
Volume Growth Rate	Slow

Table 9 Main geometry mesh settings.

Setting	Value
Base size	15 mm
Surface Growth Rate	Fast
Number of Prism Layers	5
Prism Layer Stretching	1.2
Prism Layer Total Thickness	7.5 mm
Volume Growth Rate	Medium

Table 10 Wheel mesh settings.

Setting	Value
Base size	3 mm
Surface Growth Rate	Default
Number of Prism Layers	10
Prism Layer Stretching	1.2
Prism Layer Total Thickness	12.5 mm
Volume Growth Rate	Medium

4 Results

The simulations were run until the following residuals were obtained:

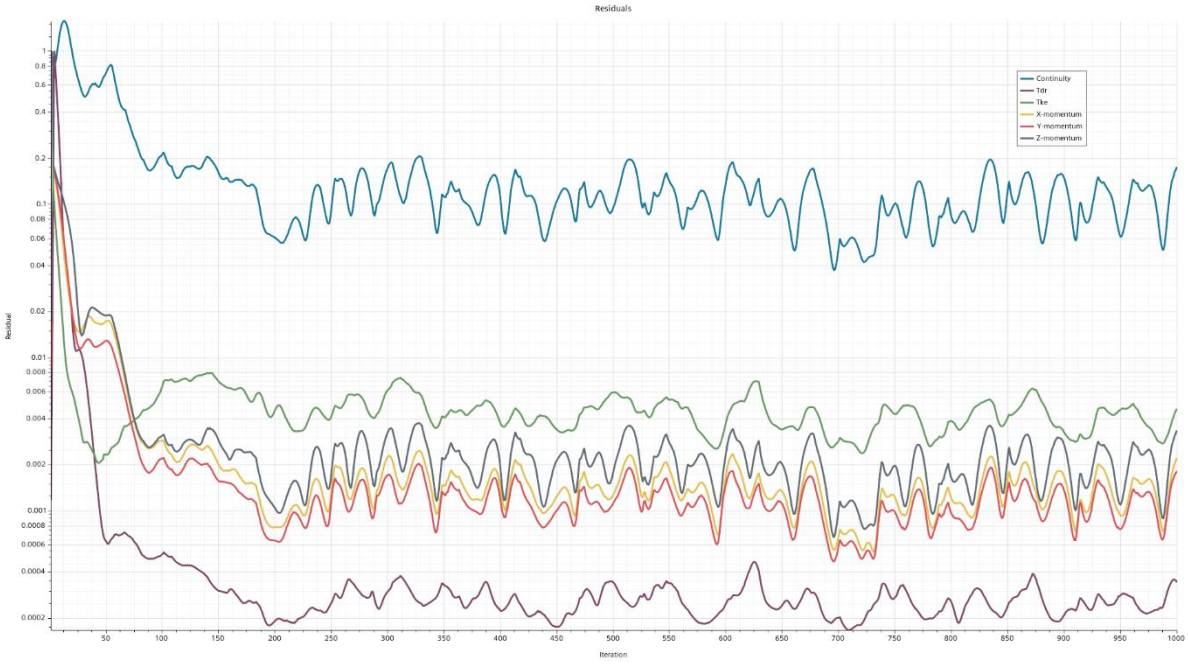

Figure 22. 2021 geometry final residuals.

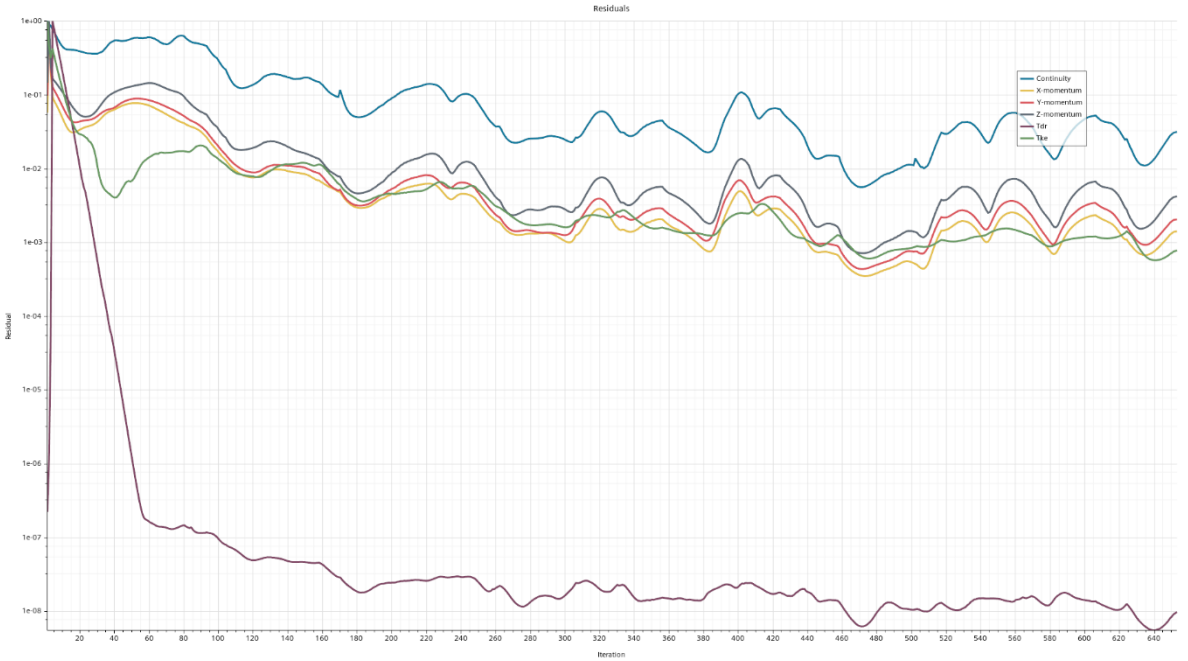

Figure 23. 2022 geometry final residuals.

The residuals do not initially appear to show convergence. However, a monitor was set for both C_L and $C_{D,}$ which converged to the values shown in section 4.1. The reason for the residual graph above is presumed to be from the transient nature of the solution. The residuals could have been oscillating like this because of the mesh resolution; however,

the simulation run on more coarse meshes also did show this pattern, so this is not the cause.

As discussed in the method, the solver used was a steady-state solver, and this was used as a compromise in computational time against the accuracy of the results. In an ideal scenario with more time and resources, a transient solver would be used to obtain a transient solution.

4.1 Lift and Drag Comparison

Table 11 Table comparing lift and drag between the geometries.

2021		2022	
C_L	C_D	C_L	C_D
0.280	0.181	0.261	0.172

This comparison was used as an indicator towards the validity of the results. The values of the coefficient of lift and drag both being higher on the 2021 car are to be expected and another sign that the results are valid and able to be analysed. The flow patterns were the main interest of this project and will be analysed in the rest of section 4.

4.2 Front Wing Flow Analysis

In this section, the flow pattern of the 2021 and 2022 front wings will be analysed using plots and isosurfaces to determine the effects of the changes in front wing geometry.

2021

The vorticity of the flow has been plotted in the figure below at three different points along the z-axis. These points are indicated on the right but are midway along the nose, at the rearmost point of the wing, and midway between the wing and wheel.

In this plot and all future plots, the vortices have been labelled and annotated for the benefit of the reader. A colour key has been provided, and any white areas of the plot are sections where the geometry intersects.

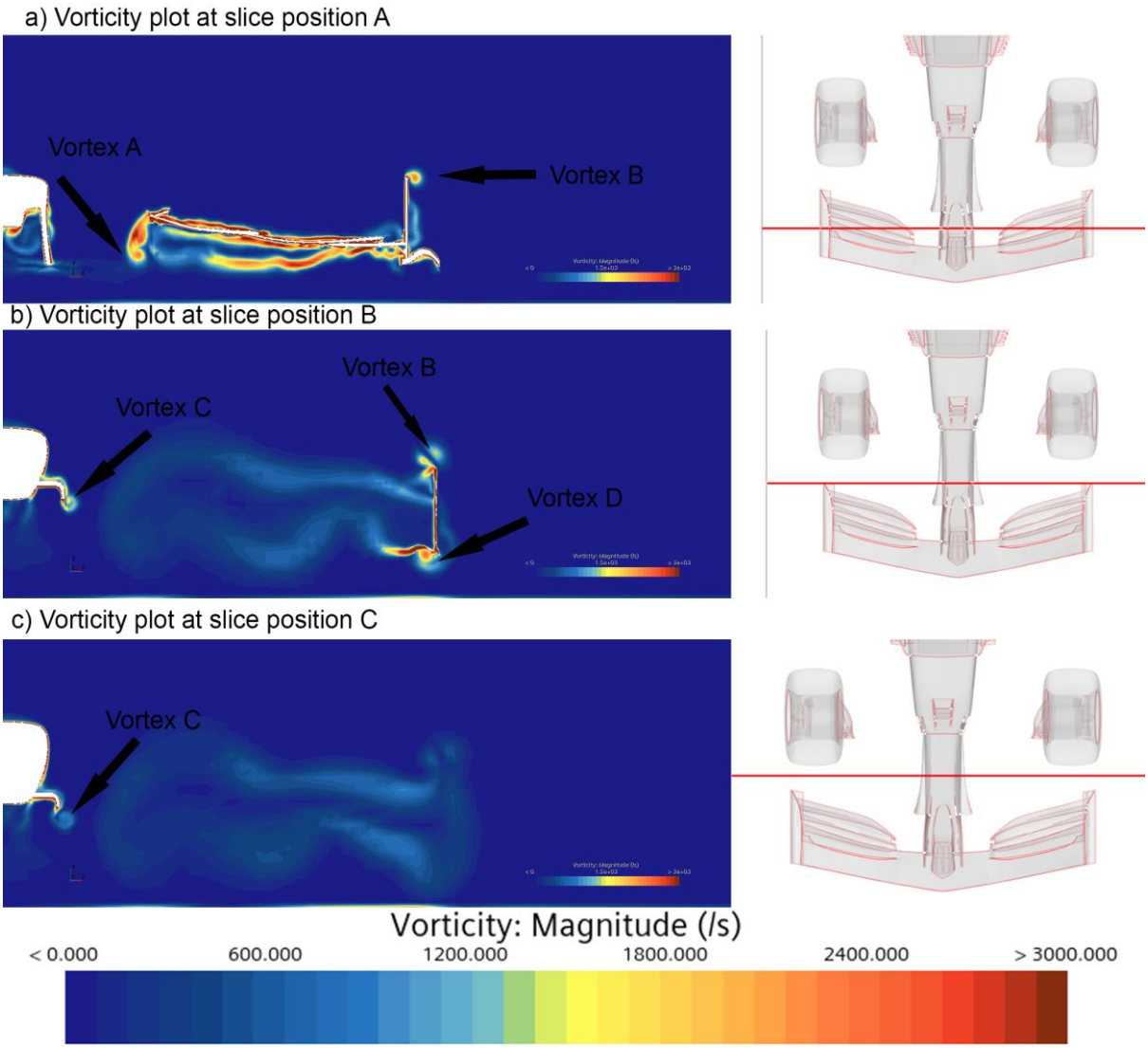

Figure 24. Vorticity plots along the 2021 front wing.

In this plot, it can be seen that there are two outboard vortices being generated (B and D). These vortices are the ones which will travel along the outside of the car, encouraging the outwash effect. Vortex B is created much further upstream compared to vortex D; however, both appear to be highly concentrated vortices with high vorticity magnitudes.

Vortex A is interesting because it appears to be the Y250 vortex. However, as can be seen in figure 24 a), the vortex is not very concentrated, making it less useful to the designers. This suggests that previous changes to the technical regulations before those being investigated in this project have also helped reduce the severity of the Y250 vortex.

Vortex C might give some insight into why the Y250 vortex is not as pronounced. Vortex C is near Vortex A, and crucially, they are counter-rotating vortices. This means that as

these flows mix, the flow will become more laminar rather than combining into one concentrated vortex.

The figure below is an isosurface showing the region of the flow with a vorticity magnitude of 300 rotations/s. Highlighted are the vortices mentioned previously, and this plot can be used to visualise the vortices in 3D to show where they flow from and to.

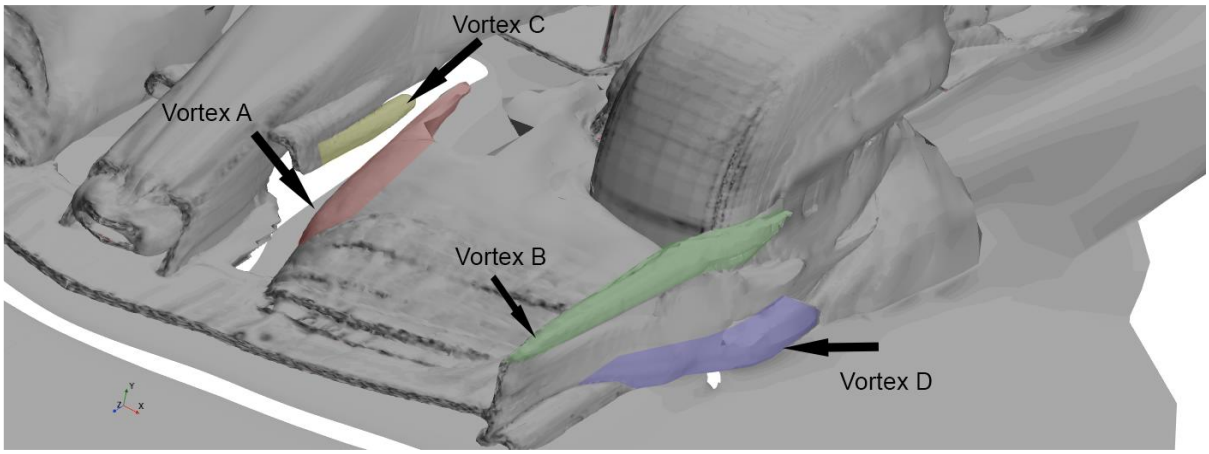

Figure 25. Vorticity isosurface of the front section of the 2021 car.

The other key finding from figure 25 is the large isosurface trailing behind the wing. This shows how turbulent the wake of the front wing is and why it is an important area to control and limit.

2022

Like 2021, the vorticity has been plotted for three different points along the front nose, and the points chosen are the same points chosen for the previous car geometry.

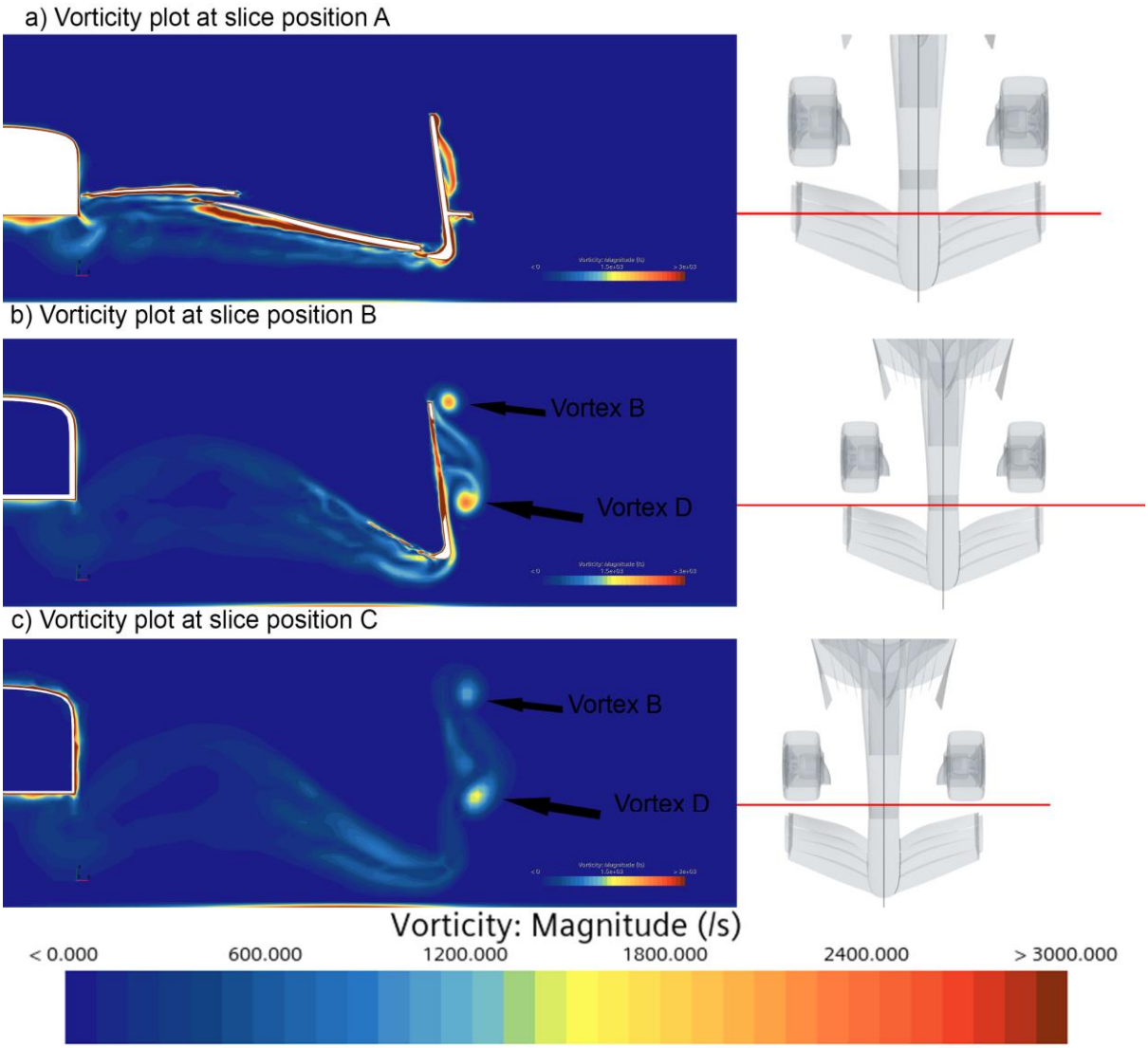

Figure 26. Vorticity plots along the 2021 front wing.

There are some very interesting findings from this plot. Firstly, vortex A and C are gone completely. This shows that the FIA's objective of eliminating the Y250 vortex has been accomplished.

The other key observation is the fact that vortex B is forming much further downstream, as vortex D did in both 2021 and 2022. The likely cause of this is the much taller front wing endplates. This delays the formation of the vortex because it is harder for the high-pressure air to spill over the top of the endplate if it is taller.

The figure below is an isosurface plot of the 2022 flow. Like 2021, it is set at 300 rotations/s.

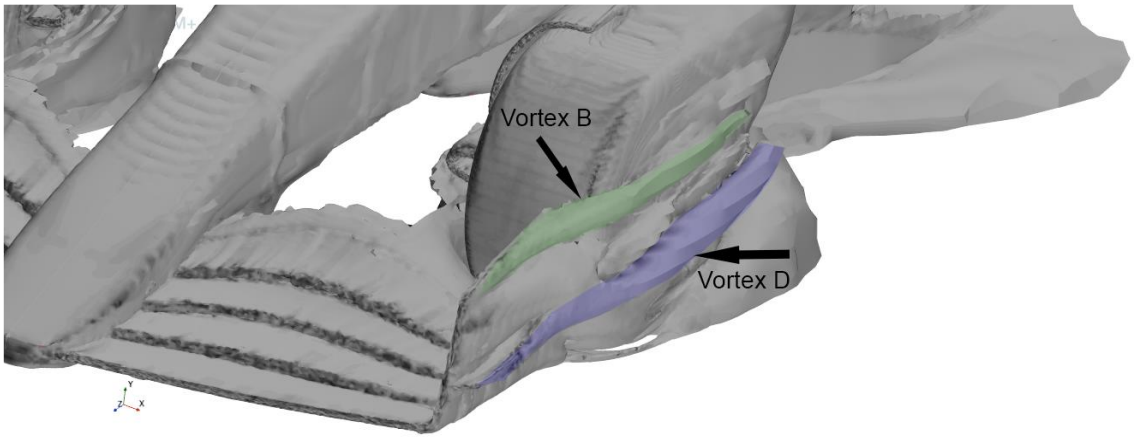

Figure 27. Vorticity isosurface of the 2022 car front section.

A comparison between figure 25 and figure 27 shows that the vortices in 2022 are much more concentrated and flow further downstream before dissipating. This has both positive and negative effects. The positive is that a more concentrated vortex means the turbulent, rotating flow occupies a smaller volume meaning more of the flow, and therefore wake of the car, is steady and laminar. However, this concentrated vortex will do a better job at encouraging outwash as a concentrated vortex can be manipulated easier by designers to achieve their goal of managing the tyre wake.

The other key point from this plot is the difference in the wake from the front wing. There is much less turbulence downstream of the front wing elements in 2022, which shows that the new camber profile of the wings achieved the objective it was introduced for.

4.2 Front Tyre Flow Analysis

This section will focus on comparing the differences in the flow around the tyres between the two sets of regulations.

2021

The figure below shows slices at the front, middle and rear of the front tyre. Figure 28 a) is the furthest upstream, and c) is the furthest downstream. There are two key findings from these plots. Firstly, in figure 28 b), it is clearly visible how the air is allowed inside the wheel rim where an extra pocket of turbulence is generated (see the arrow). There is also some flow separation at the bottom of the wheel rim, as can be seen by the lighter contours in that region.

The other point of interest is figure 28 c). This shows the size of the separation bubble behind the tyre. The separation bubble is the area enclosed by the contour lines of high vorticity.

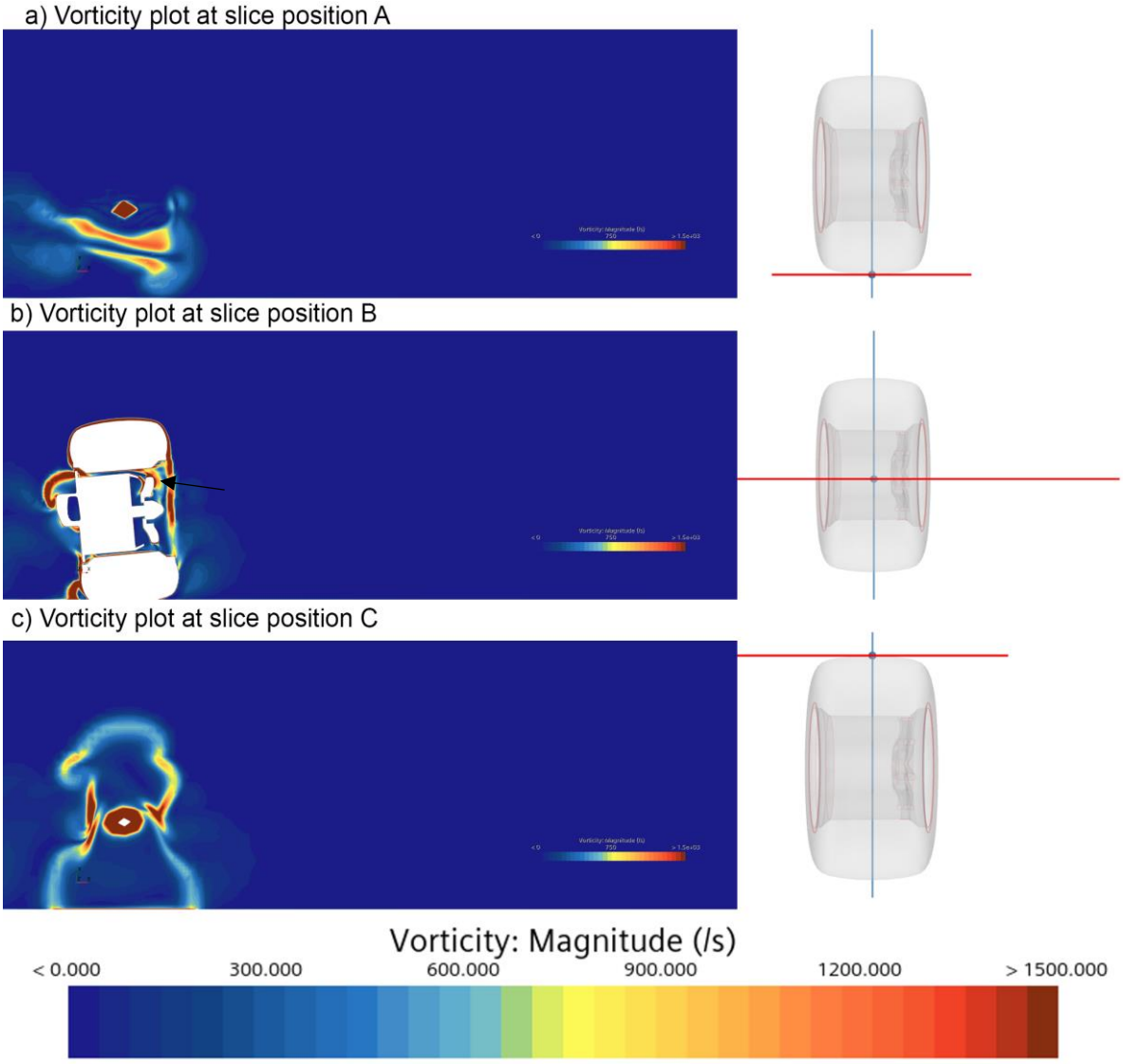

Figure 28. Vorticity plot of the flow around the 2021 front tyre.

2022

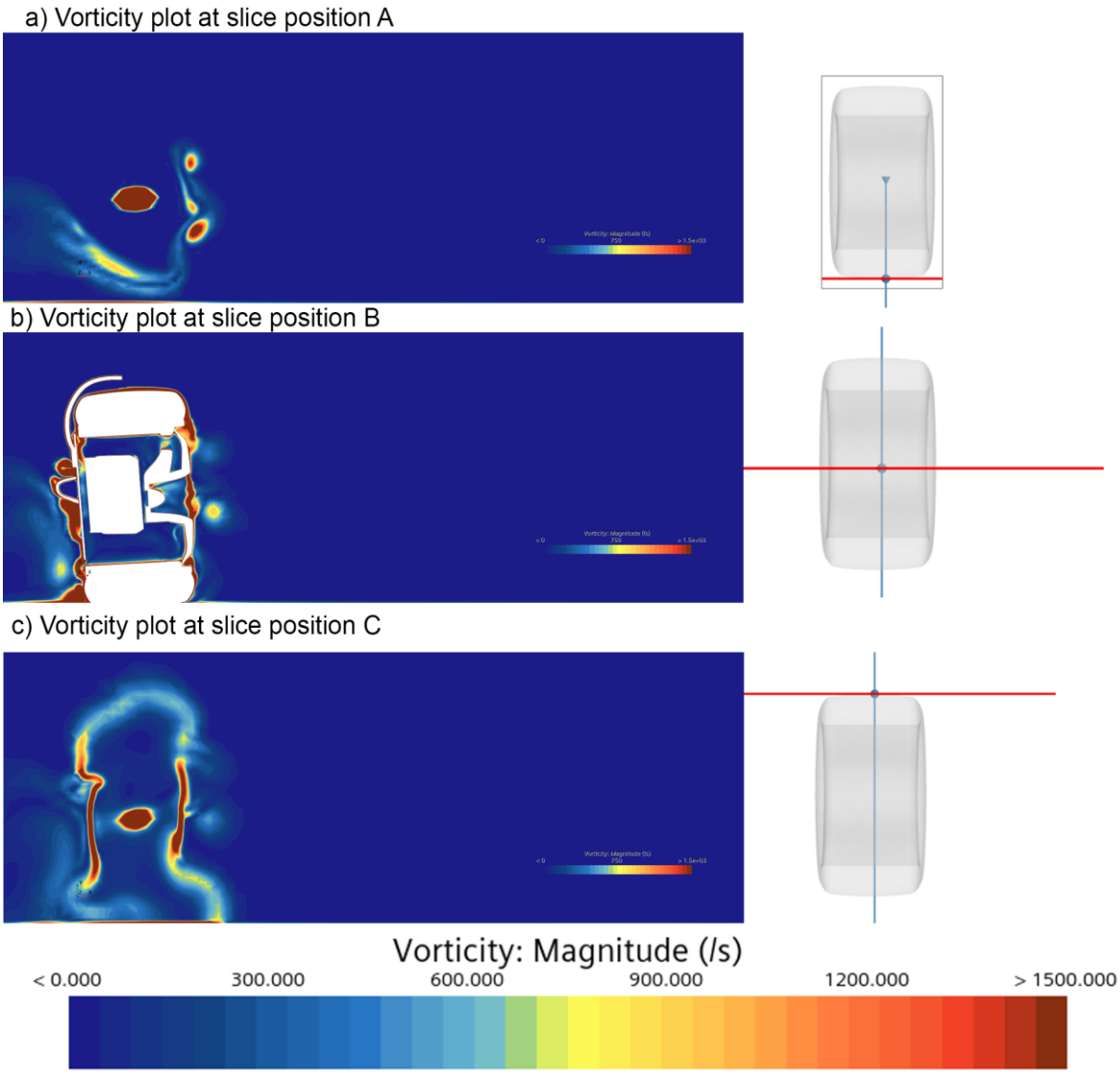

Figure 29. Vorticity plot of the flow around the 2022 front tyre.

The first key difference in this plot is in figure b). Here the benefit of the wheel rim covers can be seen as air is not allowed into the rim to be disturbed, as well as the flow stays attached to the outboard surface of the wheel.

This can be seen even better in slice C as the outboard flow has stayed better attached at the bottom of the tyre reducing the separation bubble. The size of the separation bubble is also smaller overall, and this is better demonstrated by the following C_p plot.

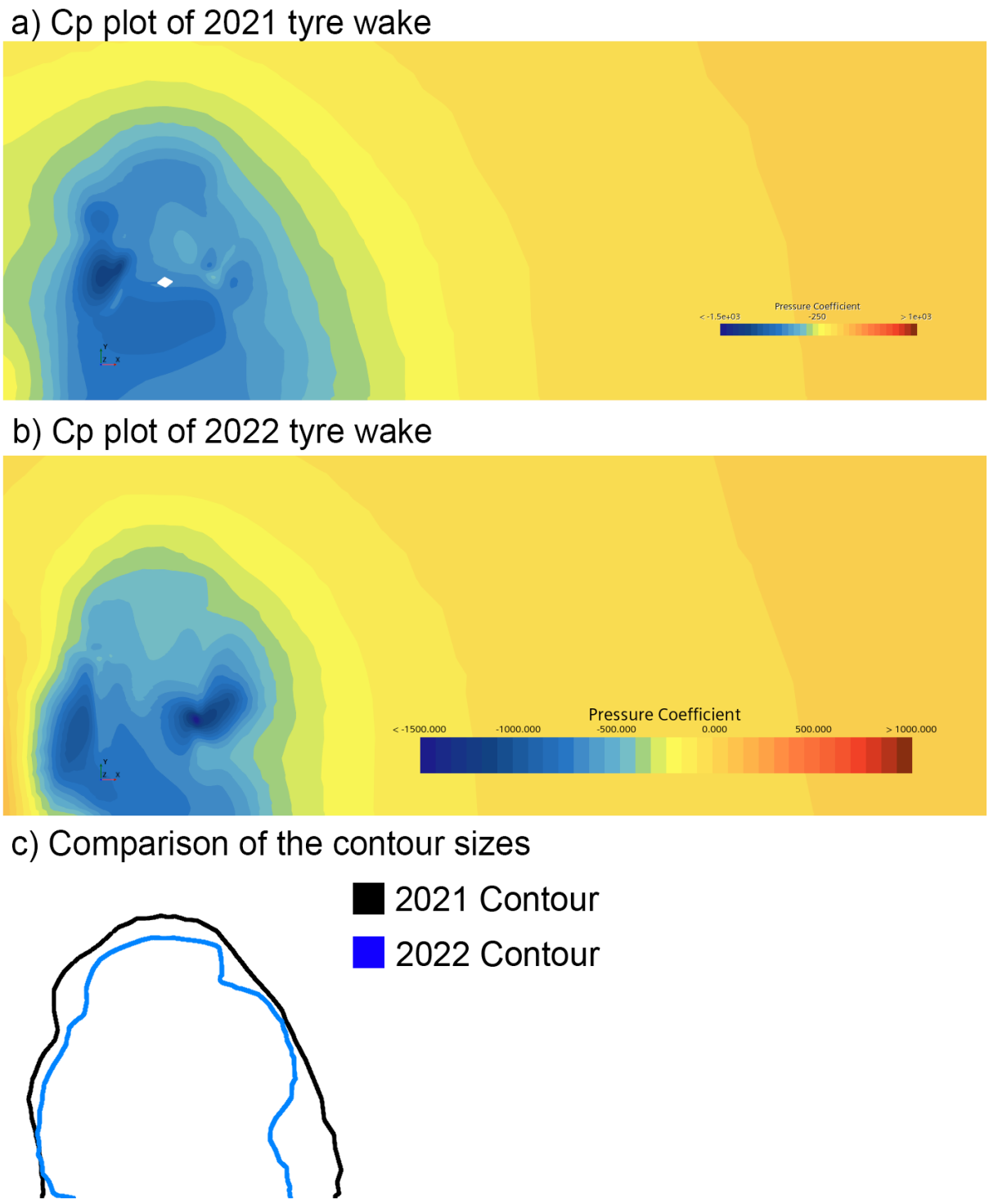

Figure 30. Comparison of the pressure distribution behind the 2021 and 2022 front tyres.

The comparison of the contour plots shows how much more the flow stays attached to the outboard section of the tyre. This can be attributed to the addition of the wheel rim covers, meaning another one of the FIA's changes appears to work.

The final check to perform was to analyse the effects of the winglet over the tyre. One interesting finding can be seen in the isosurface plot below.

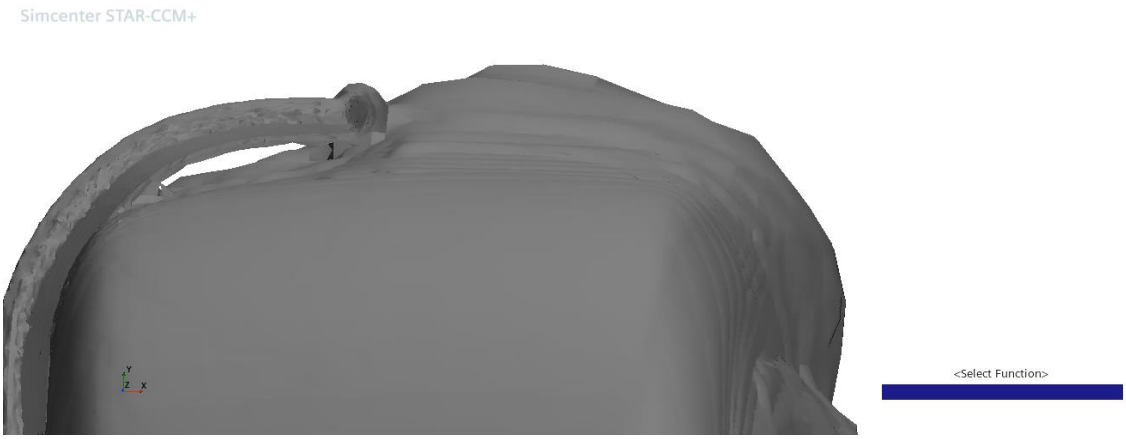

Figure 31. Isosurface of the vorticity on the top surface of the 2022 front tyre.

The isosurface shows areas of vorticity, and in the figure, the region between the winglet and tyre surface is more attached than the region that is not underneath the winglet. This is another minor reduction in the size of the separation bubble behind the tyre, which will influence reducing the turbulence of the wake. This was not something that the winglet was directly designed for, but it is positive.

The final test was to see the impact of the winglet on directing the flow. The figure below shows a set of 5 streamlines that interact with the winglet, and the flow clearly gets pushed up and outwards by the winglet, which is another successful objective met by the regulation changes.

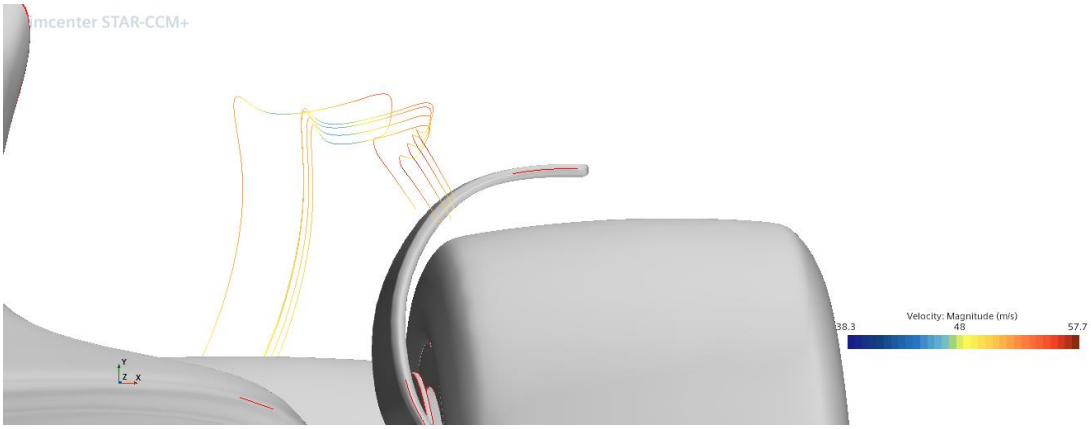

Figure 32. Streamlines of the flow around the front tyre winglet.

The biggest limitation in the tyre test, however, was the inability to simulate the deformation of the tyre under load. With the 2022 tyre rim being increased to an 18-inch diameter from 13, there should be less deformation of the tyre, meaning a more consistent flow around the tyre and less tripping of the boundary layer, which increases separation. This was not something which could be tested in this project and could have had an impact on these findings had it been.

4.3 Mid-car flow analysis

This section aims to compare the flow patterns around the mid-car section. This includes analysing the bargeboard area as well as looking at the flow along the car between the front and rear tyres.

2021

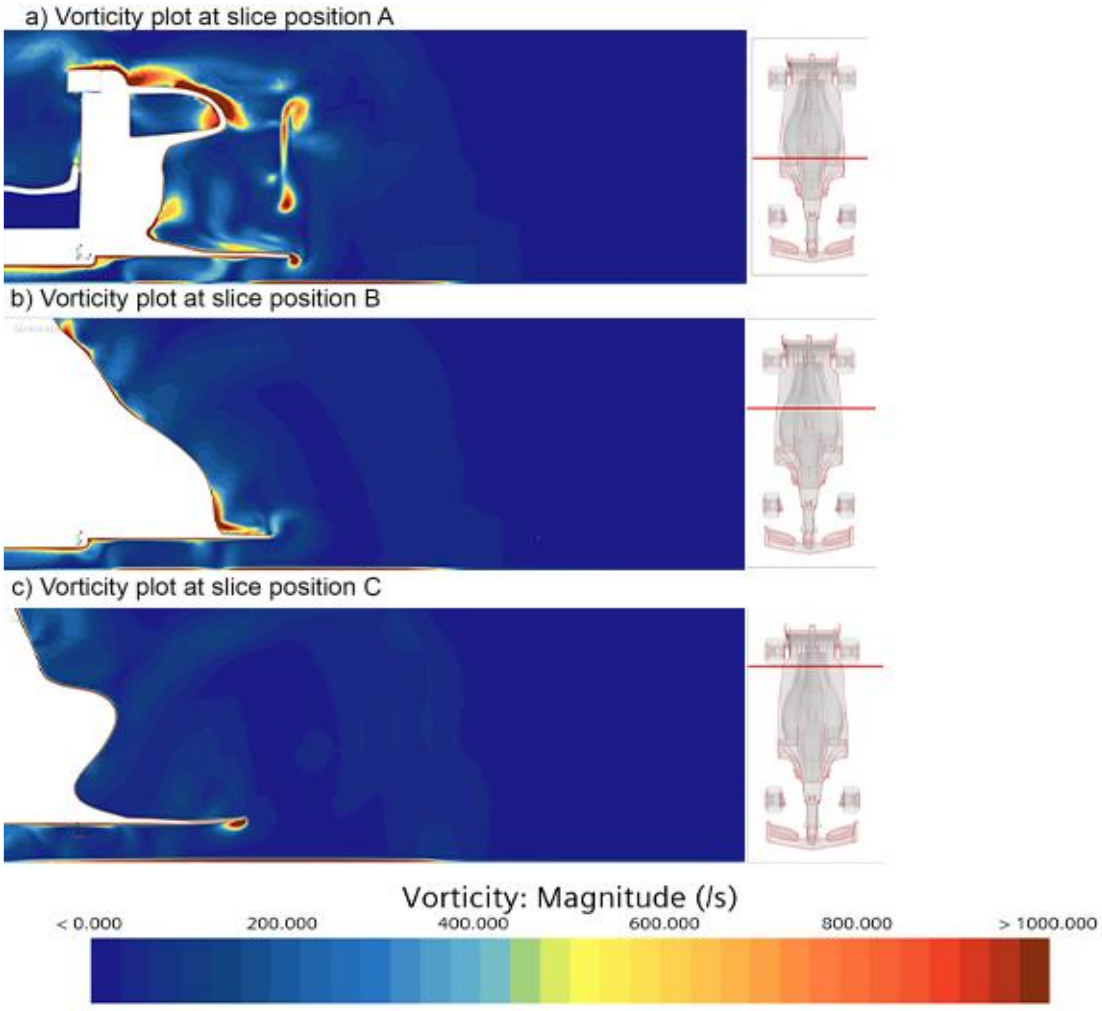

Figure 33. Plot of vorticity magnitude along the 2021 mid-car.

The plot above illustrates one key finding. There is a large amount of vorticity being shed from the bargeboards, as can be seen by the large amount of outboard vorticity in slice A, which was to be expected from the theory.

The other point of note is the vortex that is at the corner of the floor edge and is present all the way down the mid-car. This shows how the designers are trying to seal the low-pressure region under the car to keep the floor working at optimal performance.

2022

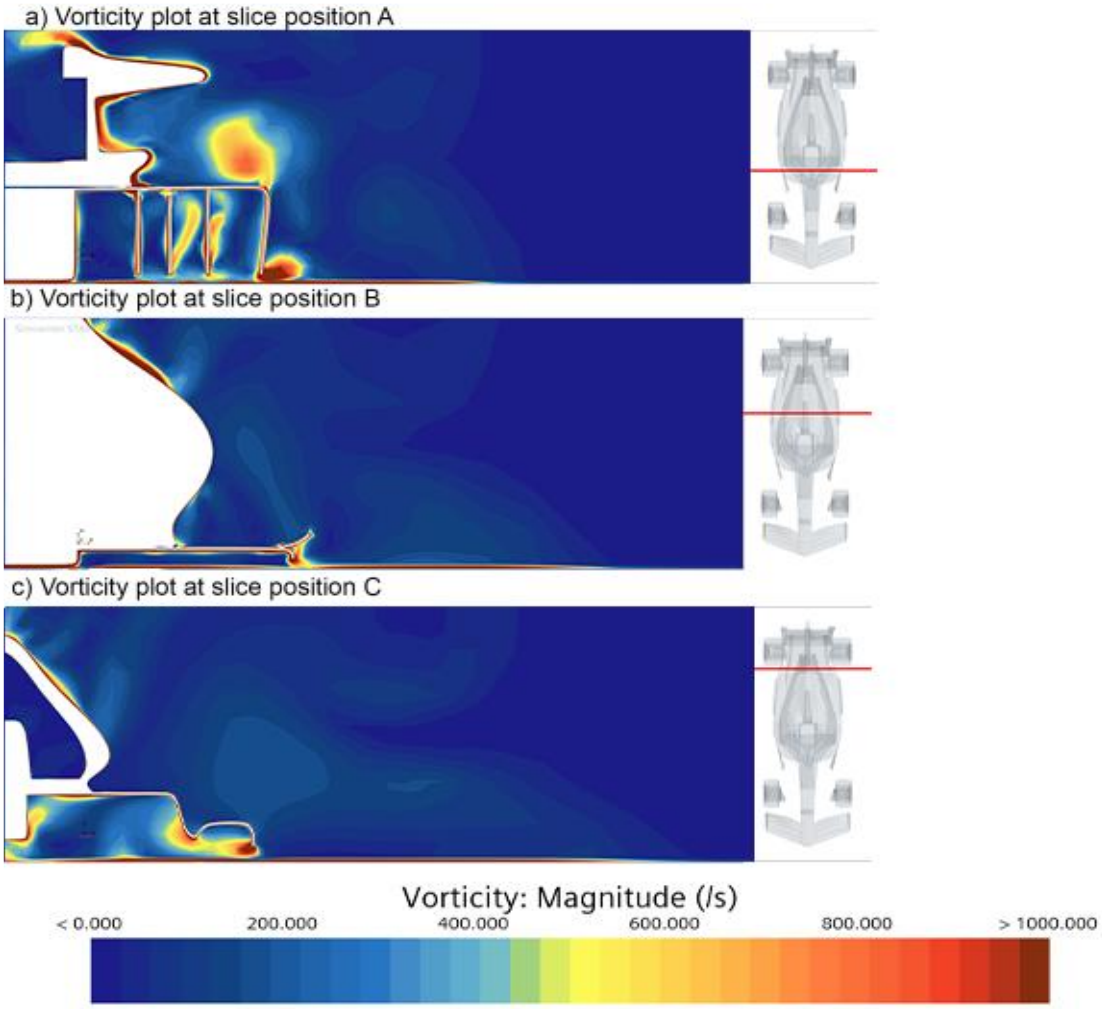

Figure 34. Plot of vorticity magnitude along the 2022 mid-car.

The key difference between 2021 and 2022 is in slice A, furthest upstream. There are not as many regions of high vorticity as in 2021; however, there is one big vortex being shed off of the top corner of the floor. It is hard to say which of these is better for the car behind from this data, so the effect of the removal of the bargeboards is inconclusive.

Crucially, the vortex sealing the floor is still present, which means the underbody should be working effectively, which is key for these new regulations to work well.

The ground effect changes were hard to model in CFD due to a lack of ride height data and the fact that the road surface would be bumpy, unlike the simulation. Additionally, the split down the centre of the car where the symmetry line may create unwanted boundary conditions, which is why an analysis of the effectiveness of the new underfloor is exempt from this investigation.

4.4 Rear Wing Analysis

This is the final section analysing the flow around individual parts, and this is a comparison of the 2021 and 2022 rear wings. This analysis will be less in-depth as the key point of interest is just the wake of the rear wing, which is shown in the figures below.

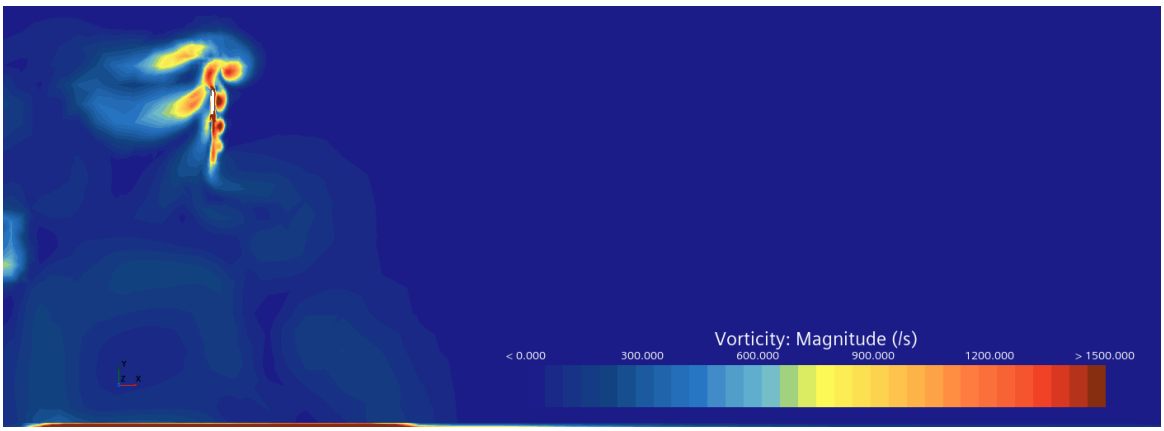

Figure 35. Vorticity plot directly behind the 2021 rear wing.

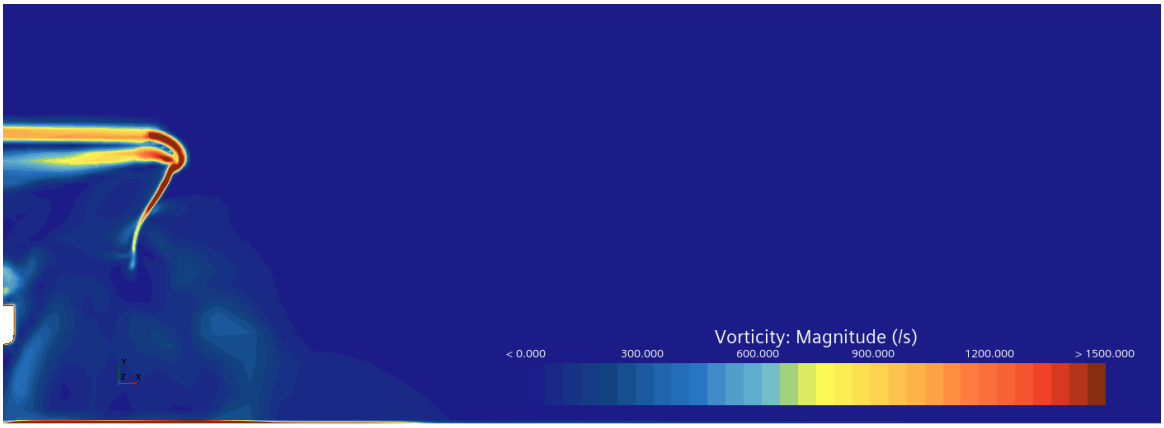

Figure 36. Vorticity plot directly behind the 2022 rear wing.

The difference between the two wings is clear. In 2021, there are five vortices being shed off the rear wing endplate, whereas 2022 shows how by removing those entirely, there is no concentrated vortex, and the only vorticity is that which comes from the flows mixing at the trailing edge of the wing. This is a huge success from the 2022 rear wing and should go a long way in improving the performance of the trailing car.

4.5 Overall Car Wake

The final analysis will be of the wake of the whole car. There will be two factors investigated: the axial velocity of the air behind the car and the amount of upwash.

Axial velocity of the wake

The axial velocity of the air along the z-axis is plotted below. The slice was positioned 0.2 m away from the floor as this is the height the front wing is positioned, and it is the part most affected by the wake of a car in front.

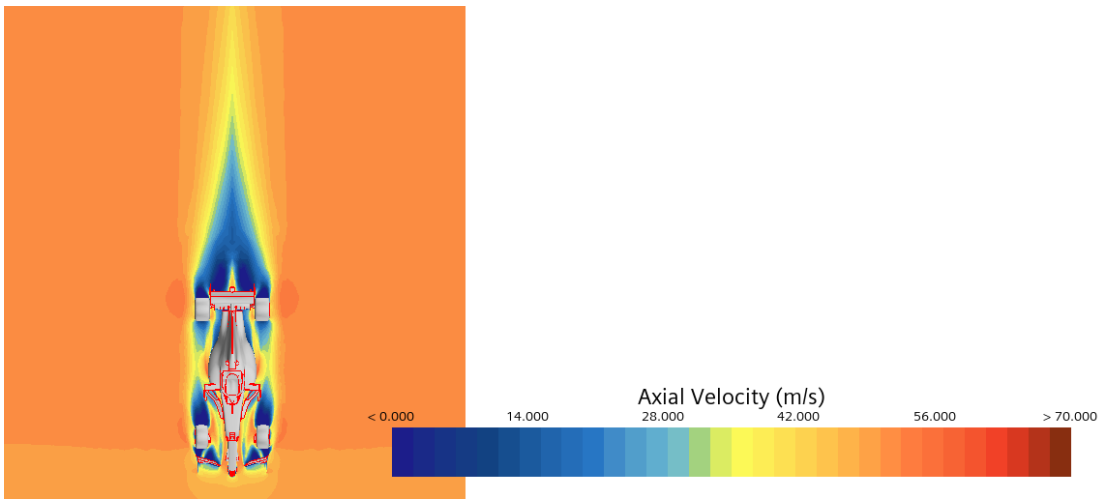

Figure 37. Plot of axial velocity in the 2021 simulation.

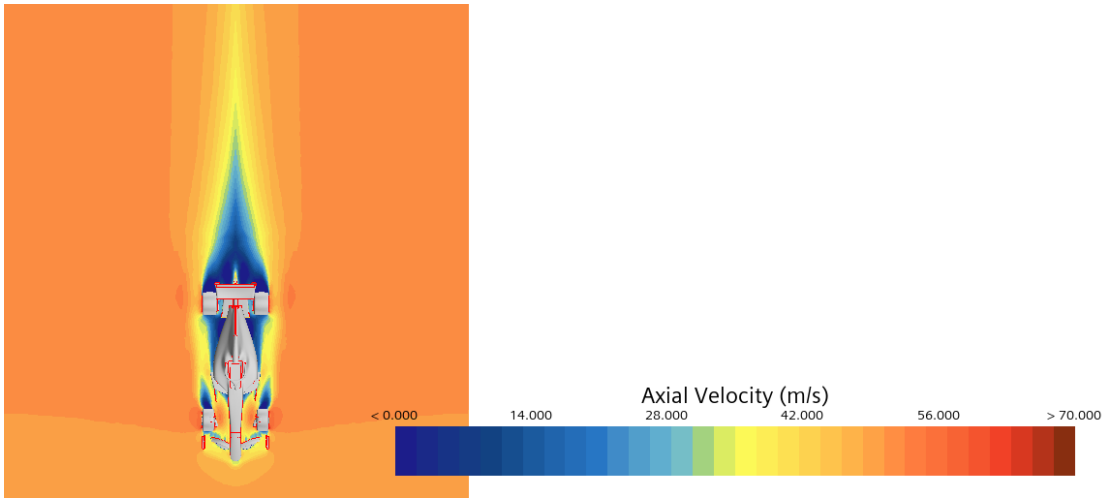

Figure 38. Plot of axial velocity in the 2022 simulation.

There is no clear difference in the flow velocity of the wake of either car. As mentioned in theory, this may ultimately be a positive as it will keep the slipstream stronger, which is a big overtaking aid. There are differences in the mid-car section. However, these are not relevant to this investigation.

Upwash

Below are 50 streamlines plotted from the floor to a height of 2 m. The source of the streamlines was the inlet for both cars, and they were positioned along the midline of the car.

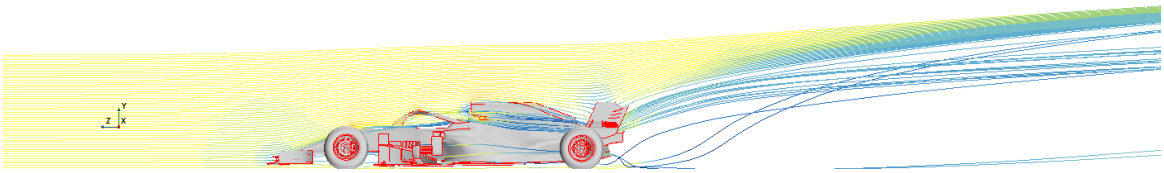

Figure 39. Streamline plot along the 2021 car.

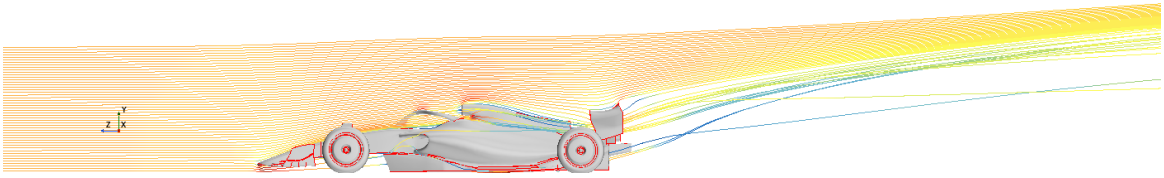

Figure 40. Streamline plot along the 2022 car.

The findings from this test were marginal. There is a very slight increase in upwash in 2022. However, it is so small that it can be deemed an insignificant increase. This is the first and only major failure found in this investigation. The 2022 car was supposed to produce a much larger amount of upwash than it seems to manage in the simulation.

5 Conclusions

This project showed promising results. It indicated that the 2022 technical regulation changes are a positive change for reducing the dirty air effect in Formula One. The front wing is shedding fewer vortices than it was before, which was a large aim of the new wing profile. The tyre wake is being reduced and managed better than it was in 2021. The removal of the bargeboard area appears to be a positive change stopping many of the concentrated vortices of 2021 from being formed. Finally, the wake of the rear wing is much less turbulent than the previous design.

On the other hand, the upwash between the two cars appears unchanged. This is probably the area which the FIA need to look at in future years if they want to build upon the changes made by these regulations.

Overall, the changes can be seen as a success. They have clearly reduced the effect of dirty air on cars following behind and should lead to better overtaking in the years to come.

6 Evaluation and Further Work

There were many limitations to this project, as have been described throughout this report. These include but are not limited to the use of a steady-state solver, the lack of modelling capabilities of the tyre deformation, outsourced geometry, and mesh quality. These have had an impact and reduced the ability to analyse the results in a quantitative manner. One next step would be to use better 3D geometry. Perhaps one modelled from scratch using photographs or, better still, building a real-life model and placing it in a wind tunnel for even better results.

In terms of other areas to investigate, the main one would be to perform analyses on a singular car and then one car following another for each of the sets of regulations and investigating the effect it has by looking at differences in lift, drag, etc.

As mentioned in the introduction, there is not a large amount of research into modern Formula One aerodynamics, and therefore, another good area would be to investigate would be isolating the various components. This would help provide more data and explanation as to how each component work which would go a long way toward increasing the amount of publicly available data surrounding Formula One.

A final idea would be to investigate the new ground effect changes closely. This report focussed on the external flow properties above the car. However, one area of interest would be comparing the performance of the two cars in an undisturbed flow to see how the changing of the regulations has affected the outright performance of the cars.

References

Anderson, G. (2022, January 25). *WHAT 2022-STYLE F1 GROUND EFFECT LOOKS LIKE*. The Race. https://the-race.com/formula-1/gary-anderson-what-2022-style-f1-ground-effect-looks-like/

Anon. (2021, December 9). *Everything we know about the 2022 F1 season: drivers, cars, tracks & more*. Autosport. https://www.motorsport.com/f1/news/2022-f1-season-drivers-cars-tracks/6868238/

Ansys. (2009). ANSYS FLUENT 12.0 User's Guide. In *Ansys, Inc.* https://www.afs.enea.it/project/neptunius/docs/fluent/html/th/node60.htm

Auto Leader. (n.d.). *How does the intriguing curved rear wing of the new F1 cars work?* Retrieved April 3, 2023, from https://moderncarsbook.com/41-how-does-the-intriguing-curved-rear-wing-of-the-new-f1-cars-work/

Camuffo, D. (2019). Chapter 1 - Microclimate and Atmospheric Variables. In D. Camuffo (Ed.), *Microclimate for Cultural Heritage (Third Edition)* (pp. 3–14). Elsevier. https://doi.org/https://doi.org/10.1016/B978-0-444-64106-9.00001-8

Croner, E., Mothay, G., Sicot, C., & Bézard, H. (2012). *Aerodynamic analysis of an isolated wheel wake*.

Dominy, J., & Dominy, R. (1984). Aerodynamic Influences on the Performance of the Grand Prix Racing Car. *Archive: Proceedings of The Institution of Mechanical Engineers, Part D: Transport Engineering 1984-1988 (Vols 198-202)*, *198*, 87–93. https://doi.org/10.1243/PIME_PROC_1984_198_134_02

Fédération Internationale de l'Automobile. (2017). *2017 FORMULA ONE TECHNICAL REGULATIONS*. https://www.fia.com/file/54257/download/18380?token=5JfbyV2g

Formula One. (2018, May 29). *TECH TUESDAY: 5 key Monaco modifications*. https://www.formula1.com/en/latest/article.tech-tuesday-5-key-monaco-modifications.1hsDGwdfHKmOeUgcMaYsaQ.html

Formula One. (2021, October 24). *FORMULA 1 ARAMCO UNITED STATES GRAND PRIX 2021 - FASTEST LAPS*. https://www.formula1.com/en/results.html/2021/races/1102/united-states/fastest-laps.html

Guerrero, A., & Castilla, R. (2020). Aerodynamic study of the wake effects on a formula 1 car. *Energies*, *13*(19). https://doi.org/10.3390/EN13195183

Guha, T. K., Oates, W., & Kumar, R. (2015). Characterization of Piezoelectric Macrofiber Composite Actuated Winglets. *Smart Materials and Structures*, *24*. https://doi.org/10.1088/0964-1726/24/6/065043

Hughes, M. (2022). *TECH TUESDAY: Why new floors should help enhance F1's wheel-to-wheel action in 2022*. Formula One. https://www.formula1.com/en/latest/article.tech-tuesday-why-new-floors-should-help-enhance-f1s-wheel-to-wheel-action-in.6WEBVH3iEhZhBvgKxTYSij.html

Hughes, M., & Piola, G. (2022). *TECH TUESDAY: How the front wing on the all-new 2022 cars has been designed to improve overtaking*. Formula One. https://www.formula1.com/en/latest/article.tech-tuesday-why-the-front-wing-will-be-a-key-technical-battleground-on-the.3Ep4LEu5mTMRkXrClOQtRg.html

Kanal, S. (2022). *IN NUMBERS: The staggering stats behind the development of the all-new 2022 car*. Formula One. https://www.formula1.com/en/latest/article.in-numbers-the-staggering-stats-behind-the-development-of-the-all-new-2022.7nYGeDoQbapwvLn1QakUAb.html

McBeath, S. (1999). *Competition Car Downforce A Practical Handbook*.

OpticalDreamSoft. (n.d.). *Professional OpticalDreamSoft 3D Models*. Retrieved February 26, 2023, from https://www.turbosquid.com/Search/Artists/OpticalDreamSoft

Red Bull Racing. (2021, February 24). *RB16B Ready To Charge After Track Debut*. https://www.redbull.com/int-en/redbullracing/rb16b-track-debut

Reynolds, J. (2021). *ANALYSIS: Comparing the key differences between the 2021 and 2022 F1 car designs*. Formula One. https://www.formula1.com/en/latest/article.analysis-comparing-the-key-differences-between-the-2021-and-2022-f1-car.4xYDhtOjDee4cEQ3P4RsK9.html

Scarborough, C. (2021). *F1 TV Tech Talk: How will the 2022 F1 car improve overtaking?* Formula One. https://www.formula1.com/en/latest/article.tech-tuesday-why-the-front-wing-will-be-a-key-technical-battleground-on-the.3Ep4LEu5mTMRkXrClOQtRg.html

Umberto Ravelli, & Marco Savini. (2018). Aerodynamic Simulation of a 2017 F1 Car with Open-Source CFD Code. *Journal of Traffic and Transportation Engineering*, *6*(4). https://doi.org/10.17265/2328-2142/2018.04.001

wickedender. (2013, November 23). *RB9 Formula 1 car front wing vortices.* https://www.youtube.com/watch?v=ZlDnd3B1rhs

Zhang, X., Toet, W., & Zerihan, J. (2006). Ground Effect Aerodynamics of Race Cars. *Applied Mechanics Reviews*, *59*(1), 33–49. https://doi.org/10.1115/1.2110263

Zhang, Z., Wang, Z., & Gursul, I. (2022). Aerodynamics of a wing in turbulent bluff body wakes. *Journal of Fluid Mechanics*, *937*, A37. https://doi.org/DOI: 10.1017/jfm.2022.132